Soft-core meson-baryon interactions. II. πN and K^+N scattering

H. Polinder[1,2] and Th. A. Rijken[1]
[1]*Institute for Theoretical Physics, Radboud University Nijmegen, Nijmegen, The Netherlands*
[2]*Forschungszentrum Jülich, Institut für Kernphysik (Theorie), D-52425 Jülich, Germany*
(Received 30 May 2005; published 30 December 2005)

The πN potential includes the t-channel exchanges of the scalar mesons σ and f_0, vector meson ρ, tensor mesons f_2 and f_2', and the Pomeron as well as the s- and u-channel exchanges of the nucleon N and the resonances Δ, Roper, and S_{11}. These baryonic resonances are not generated dynamically. We consider them, at least partially, as genuine three-quark states, and we treat them in the same way as the nucleon. The Roper and S_{11} resonances were needed to find the proper behavior of the phase shifts at higher energies in the corresponding partial waves. The soft-core πN model gives an excellent fit to the empirical πN S- and P-wave phase shifts up to $T_{\rm lab} = 600$ MeV. Also, the scattering lengths have been reproduced well, and the soft-pion theorems for low-energy πN scattering are satisfied. The soft-core model for the K^+N interaction is an $\mathrm{SU}_f(3)$ extension of the soft-core πN model. The K^+N potential includes the t-channel exchanges of the scalar mesons a_0, σ, and f_0, vector mesons ρ, ω, and ϕ, tensor mesons a_2, f_2, and f_2', and the Pomeron as well as u-channel exchanges of the hyperons Λ, Σ, $\Sigma(1385)$, and $\Lambda(1405)$. The fit to the empirical K^+N S-, P-, and D-wave phase shifts up to $T_{\rm lab} = 600$ MeV is reasonable and certainly reflects the present state of the art. Since the various K^+N phase shift analyses are also not very consistent, scattering observables are also compared with the soft-core K^+N model. A good agreement for the total and differential cross sections as well as the polarizations is found.

DOI: 10.1103/PhysRevC.72.065211 PACS number(s): 12.39.Pn, 21.30.−x, 13.75.Gx, 13.75.Jz

I. INTRODUCTION

In the previous paper (paper I) [1], the Nijmegen soft-core (NSC) model for the pseudoscalar-meson-baryon interaction in general is derived. In this paper (paper II), we apply the NSC model to the πN and K^+N interactions.

The interaction between a pion and a nucleon has been investigated experimentally as well as theoretically for many years. For the early literature, we would like to refer to Chew and Low [2] (who presented one of the best early models that successfully described the low-energy P-wave scattering), Hamilton [3], Bransden and Moorhouse [4], and Höhler [5].

Although the underlying dynamics of strong hadron interactions in general and the πN interaction specifically are believed to be given by quark-gluon interactions (QCD), it is in principle not possible to use *ab initio* these degrees of freedom to describe the strong low- and intermediate-energy interactions. This problem is related to the phase transition between strong low- and high-energy interactions and the nonperturbative nature of confinement. Instead, an effective theory with meson and baryon degrees of freedom must be used to describe strong interaction phenomena at low and intermediate energies; at these energies, the detailed quark-gluon structure of hadrons is expected to be unimportant.

In particular, meson-exchange models have proven to be very successful in describing the low- and intermediate-energy baryon-baryon interactions for the NN and YN channels [6,7]. Similarly, it is expected that this approach can also be successfully applied to the meson-baryon sector, i.e., πN, K^+N, K^-N, etc.

In the last decade, the low- and intermediate-energy πN interaction has been studied theoretically, analogous to the NN interaction, in the framework of meson and baryon exchange by several authors [8–14]. The K^+N interaction has been investigated in this framework only by the Jülich group [15,16] and in this work. In the same way as the Nijmegen soft-core YN model was derived in the past as an $\mathrm{SU}_f(3)$ extension of the Nijmegen soft-core NN model, we present the NSC K^+N model as an $\mathrm{SU}_f(3)$ extension of the NSC πN model.

The above πN meson-exchange models have in common that not only the nucleon pole terms but also the $\Delta_{33}(1232)$ (Δ) pole terms are included explicitly; i.e., the Δ is not considered to be purely dynamically generated as a quasibound πN state, which might be possible if the πN potential is sufficiently attractive in the P_{33} wave. This possibility was investigated in the past by Ref. [17]. From the quark model point of view, the Δ resonance and other resonances are fundamental three-quark states and should be treated the same as nucleons.

We remark that the exact treatment of the propagator of the Δ and its coupling to πN is different in each model. The NSC πN model uses the same coupling and propagator for Δ as that of Schütz *et al.* [10].

The above πN models differ, however, in the treatment of the other resonances, $P_{11}(1440)$ (Roper or N^*), $S_{11}(1535)$, etc. Gross and Surya [9] include the Roper resonance explicitly, but the $S_{11}(1535)$ resonance is generated dynamically in their model, which gives a good description of the experimental data up to $T_{\rm lab} = 600$ MeV. Schütz *et al.* [10] do not include the Roper resonance explicitly but generate it dynamically. However, their model describes the πN data only up to $T_{\rm lab} = 380$ MeV; and in this energy region, the Roper is not expected to contribute much. Pascalutsa and Tjon [13] include the above resonances explicitly in their model in order to find a proper description of the experimental data up to $T_{\rm lab} = 600$ MeV. The resonances that are relevant in the energy region we consider, the Δ, Roper, and $S_{11}(1535)$, are included explicitly in the NSC πN model.

Several other approaches to the πN interaction can be found in the literature; quark models have been used to describe πN scattering [18]. Also, models in the framework of chiral perturbation theory exist [19,20]; however, heavier degrees of freedom, such as vector mesons, are integrated out in this framework. We do not integrate out these degrees of freedom, but include them explicitly in the NSC model.

For the πN interaction, accurate experimental data exist over a wide energy range, and both energy-dependent and energy-independent phase shift analyses of that data have been made, e.g., Refs. [21–24]. Several partial wave analyses for the πN interaction as well as for other interactions are available at http://gwdac.phys.gwu.edu/ (SAID, which is run by the CNS Data Analysis Center at George Washington University).

There is an important difference between the kaon (K)- or antikaon ($\bar{K}$)- and the pion-nucleon interactions. This is due to the difference in strangeness, which is conserved in strong interactions. Kaons have strangeness $S = 1$, meaning that they contain an $\bar{s}$ quark and a u or d quark in case of K^+ and K^0, respectively. Antikaons have strangeness $S = -1$, meaning that they contain an s quark and a $\bar{u}$ or $\bar{d}$ quark in case of K^- and $\bar{K}^0$, respectively. Since the $\bar{u}$ or $\bar{d}$ quark of the antikaon can annihilate with a u or d quark of the nucleon, the $\bar{K}N$ interaction is strong because low-lying Λ and Σ resonances can be produced, giving a large cross section. This situation can be compared with the Δ resonance in πN interactions.

The $\bar{s}$ quark of the kaon cannot annihilate with one of the quarks of the nucleon in strong interactions; therefore, three-quark resonances cannot be produced, only heavy exotic five-quark ($qqqq\bar{q}$) resonances (referred to as Z^* in the old literature or the pentaquark Θ^+ in the new literature) can be formed. So the K^+N interaction is weak at energies below the energy of Z^*, the cross sections are not large, and the S-wave phase shifts are repulsive.

However, in four recent photoproduction experiments [25] indications are found for the existence of a narrow exotic $S = 1$ light resonance in the $I = 0$ K^+N system with $\sqrt{s} \simeq 1540$ MeV and $\Gamma \leqslant 25$ MeV. The existence of such an exotic resonance was predicted by Diakonov *et al*. [26]; they predicted the exotic resonance to have a mass of about 1530 MeV, width of less than 15 MeV, and spin-parity $J^P = \frac{1}{2}^+$.

The existing K^+N scattering data, which we use to fit the NSC K^+N model, however, does not show this low-lying exotic resonance. On the other hand, this exotic resonance has not been searched for at low energies in the scattering experiments. At these energies, not much scattering data exist and a narrow resonance could have escaped detection.

For the early literature on the K^+N interaction, we refer to the review article by Dover and Walker [27]. The K^+N interaction has been studied by the Jülich group, (Bütgen *et al*. [15] and Hoffmann *et al*. [16]), and they presented a model in the meson-exchange framework, analogous to the Bonn NN model [7].

In Ref. [15], a reasonable description of the empirical phase shifts is obtained; here not only single-particle exchanges [σ, ρ, ω, Λ, Σ, $\Sigma(1385)$] are included in the K^+N model, but also fourth-order processes with N, Δ, K, and K^* intermediate states are included in analogy to the Bonn NN model, in which σ exchange effectively represents correlated two-pion exchange. Coupling constants involving strange particles are obtained from the known $NN\pi$ and $\pi\pi\rho$ coupling constants assuming SU(6) symmetry.

However, an exception had to be made for the ω coupling, which had to be increased by 60% in order to find enough short-range repulsion and to obtain a reasonable description of the S-wave, phase shifts, model A. But this also caused too much repulsion in the higher partial waves, and it was concluded that the necessary repulsion had to be of much shorter range. In model B, the ω coupling was kept at its symmetry value and a phenomenological short-range repulsive σ_0 with a mass of 1200 MeV was introduced, which led to a more satisfactory description of the empirical phase shifts.

In Ref. [16], the model of Ref. [15] is extended by replacing the σ and ρ exchange by the correlated two-pion exchange. A satisfactory description of the experimental observables up to $T_{\rm lab} = 600$ MeV, having the same quality as in Ref. [15], is achieved. Just as in Ref. [15], the phenomenological short-range σ_0 was needed in this model in order to keep the ω coupling at its symmetry value. Bütgen *et al*. suggest that this short-range σ_0 might be seen as a real scalar meson or perhaps as a real quark-gluon effect.

The most recent quark models for the K^+N interaction are from Barnes and Swanson [28], Silvestre-Brac *et al*. [29], and Lemaire *et al*. [30]. The agreement of these quark models with the experimental data is not good. The results of Refs. [29,30] show that there is enough repulsion in the S waves, but the other waves cannot be described well.

Recently, a hybrid model for the K^+N interaction was published by Hadjimichef *et al*. [31]. They used the Jülich model extended by the inclusion of the isovector scalar-meson $a_0(980)$ exchange, which was taken into account in the Bonn NN model [7], but not in the Jülich K^+N models [15,16]. The short-range phenomenological σ_0 exchange was replaced by quark-gluon exchange. A nonrelativistic quark model, which considers a one-gluon exchange and the interchange of the quarks, was used. This quark-gluon exchange is, contrary to the σ_0 exchange, isospin dependent. A satisfactory description of the empirical phase shifts, having the same quality as [16], was obtained. However, Hadjimichef *et al*. conjecture that the short-range quark-gluon dynamics they include could perhaps be replaced by the exchange of heavier vector mesons.

Another approach for the K^+N interaction is given by Lutz and Kolomeitsev [20], who studied meson-baryon interactions in general and K^+N interactions specifically by means of chiral Lagrangians. A reasonable description of the K^+N differential cross sections and phases was achieved, but only up to $T_{\rm lab} = 360$ MeV.

The major differences between the existing πN and K^+N models and the NSC model presented in this work are briefly discussed below. Form factors of the Gaussian type are used in the soft-core approach in this work, while monopole-type form factors and other form factors are used for the πN model by Pascalutsa and Tjon [13] and the K^+N model by Hoffmann *et al*. [16]. The Roper resonance in the πN system is at least partially considered as a three-quark state, treated in the same way as the nucleon, and included explicitly in the potential. However, we renormalize the Roper contribution at its pole,

while Pascalutsa and Tjon [13] renormalize it at the nucleon pole.

Another difference is our treatment of the scalar mesons σ, etc.; we consider them as belonging to an $SU_f(3)$ nonet, while all other models consider them as representing effectively a correlated two-pion exchange. Also, we include the Pomeron exchange, where the physical nature of the Pomeron can be seen in light of QCD as (partly) a two-gluon-exchange effect [32] in order to comply with the soft-pion theorems for low-energy πN scattering [33,34]. Furthermore, the exchange of tensor mesons is included in the NSC model mainly to find a good description of the K^+N scattering data. We use only one-particle exchanges to find this description, while Hoffmann *et al*. [16] need to consider two-particle exchanges in their K^+N model.

The contents of this paper are as follows. In Sec. II, the $SU_f(3)$ relations between the coupling constants used in the πN and K^+N interactions are shown. The πN total cross section shows several resonances in the considered energy range. The renormalization procedure we use to include the s-channel Feynman diagrams for the resonances in the πN potential is described in Sec. III. In Sec. IV, the NSC πN model is discussed and the results of the fit to the empirical phase shifts of the lower partial waves are presented. The NSC πN model is, via $SU_f(3)$ symmetry, extended to the NSC K^+N model in Sec. V. The results of the fit to the empirical phase shifts are given, since the different phase shift analyses are not always consistent; also, the model calculation of some scattering observables is given. The NSC K^+N model is used to obtain a theoretical estimate for the upper limit of the decay width of the recently discovered exotic resonance in the isospin-zero K^+N system.

Finally, the summary presents an overview of the research in this work, its main results, and some suggestions for improvement and extension of the present NSC model. Appendix A provides details on the calculation of the isospin factors for πN and K^+N interactions.

II. MESON-BARYON CHANNELS AND $SU_f(3)$

We consider in this work the πN and K^+N interactions, which make up only a subset of all the meson-baryon interactions. Because the NSC K^+N model is derived from the NSC πN model, using $SU_f(3)$ symmetry, we define an $SU_f(3)$ invariant interaction Hamiltonian describing the baryon-baryon-meson and meson-meson-meson vertices. The Lorentz structure of the baryon-baryon-meson interaction is discussed in paper I; here, we deal with its $SU_f(3)$ structure. In order to describe the interaction Hamiltonian, we define the octet irreducible representation (irrep) of $SU_f(3)$ for the $J^P = \frac{1}{2}^+$ baryons and the octet and singlet irreducible representations of $SU_f(3)$ for the mesons. Using the phase convention of Ref. [35], the $J^P = \frac{1}{2}^+$ baryon octet irrep can be written as the traceless 3×3 matrix

$$\mathcal{B} = \begin{pmatrix} \frac{\Sigma^0}{\sqrt{2}} + \frac{\Lambda}{\sqrt{6}} & \Sigma^+ & p \\ \Sigma^- & -\frac{\Sigma^0}{\sqrt{2}} + \frac{\Lambda}{\sqrt{6}} & n \\ -\Xi^- & \Xi^0 & -\frac{2\Lambda}{\sqrt{6}} \end{pmatrix}. \tag{2.1}$$

Similarly, the pseudoscalar-meson octet irrep can be written as

$$\mathcal{P}_8 = \begin{pmatrix} \frac{\pi^0}{\sqrt{2}} + \frac{\eta_8}{\sqrt{6}} & \pi^+ & K^+ \\ \pi^- & -\frac{\pi^0}{\sqrt{2}} + \frac{\eta_8}{\sqrt{6}} & K^0 \\ K^- & K^0 & -\frac{2\eta_8}{\sqrt{6}} \end{pmatrix}, \tag{2.2}$$

while the pseudoscalar-meson singlet irrep is the 3×3 diagonal matrix $\mathcal{P}_1$ with the elements $\eta_1/\sqrt{3}$ on the diagonal. The pseudoscalar-meson nonet, having a nonzero trace, is given by

$$\mathcal{P} = \mathcal{P}_8 + \mathcal{P}_1. \tag{2.3}$$

The physical mesons η and η' are superpositions of the octet and singlet mesons η_8 and η_1, usually written as

$$\begin{aligned} \eta' &= \sin\theta\eta_8 + \cos\theta\eta_1, \\ \eta &= \cos\theta\eta_8 - \sin\theta\eta_1. \end{aligned} \tag{2.4}$$

Similar expressions hold for the physical coupling constant of the η and η'. The octets and singlets for the scalar and vector mesons are defined in the same way, and the expressions for the physical (ω, ϕ) and (σ, f_0) are analogous to (η', η). From these octets and nonets, the $SU_f(3)$-invariant baryon-baryon-meson interaction Hamiltonians can be constructed, using the invariants $\mathrm{Tr}(\bar{\mathcal{B}}\mathcal{P}\mathcal{B})$, $\mathrm{Tr}(\bar{\mathcal{B}}\mathcal{B}\mathcal{P})$, and $\mathrm{Tr}(\bar{\mathcal{B}}\mathcal{B})\mathrm{Tr}(\mathcal{P})$. Taking the antisymmetric (F) and symmetric (D) octet couplings and the singlet (S) coupling, we obtain

$$\begin{aligned} [\bar{\mathcal{B}}\mathcal{B}\mathcal{P}]_F &= \mathrm{Tr}(\bar{\mathcal{B}}\mathcal{P}\mathcal{B}) - \mathrm{Tr}(\bar{\mathcal{B}}\mathcal{B}\mathcal{P}) \\ &= \mathrm{Tr}(\bar{\mathcal{B}}\mathcal{P}_8\mathcal{B}) - \mathrm{Tr}(\bar{\mathcal{B}}\mathcal{B}\mathcal{P}_8), \\ [\bar{\mathcal{B}}\mathcal{B}\mathcal{P}]_D &= \mathrm{Tr}(\bar{\mathcal{B}}\mathcal{P}\mathcal{B}) + \mathrm{Tr}(\bar{\mathcal{B}}\mathcal{B}\mathcal{P}) - \tfrac{2}{3}\mathrm{Tr}(\bar{\mathcal{B}}\mathcal{B})\mathrm{Tr}(\mathcal{P}) \\ &= \mathrm{Tr}(\bar{\mathcal{B}}\mathcal{P}_8\mathcal{B}) + \mathrm{Tr}(\bar{\mathcal{B}}\mathcal{B}\mathcal{P}_8), \\ [\bar{\mathcal{B}}\mathcal{B}\mathcal{P}]_S &= \mathrm{Tr}(\bar{\mathcal{B}}\mathcal{B})\mathrm{Tr}(\mathcal{P}) = \mathrm{Tr}(\bar{\mathcal{B}}\mathcal{B})\mathrm{Tr}(\mathcal{P}_1). \end{aligned} \tag{2.5}$$

The $SU_f(3)$-invariant baryon-baryon-meson interaction Hamiltonian is a linear combination of these quantities and defined according to [35] as

$$\begin{aligned} m_{\pi^+}\mathcal{H} = {} & f_8\sqrt{2}(\alpha[\bar{\mathcal{B}}\mathcal{B}\mathcal{P}]_F + (1-\alpha)[\bar{\mathcal{B}}\mathcal{B}\mathcal{P}]_D) \\ & + f_1\sqrt{\frac{1}{3}}[\bar{\mathcal{B}}\mathcal{B}\mathcal{P}]_S. \end{aligned} \tag{2.6}$$

Here, α is the $F/(F+D)$ ratio. The most general interaction Hamiltonian that is invariant under isospin transformations is given by

$$\begin{aligned} m_{\pi^+}\mathcal{H}_1 = {} & [f_{NN\eta_1}(\bar{N}N) + f_{\Lambda\Lambda\eta_1}(\bar{\Lambda}\Lambda) + f_{\Sigma\Sigma\eta_1}(\bar{\boldsymbol{\Sigma}}\cdot\boldsymbol{\Sigma}). \\ & + f_{\Xi\Xi\eta_1}(\bar{\Xi}\Xi)]\eta_1, \\ m_{\pi^+}\mathcal{H}_8 = {} & f_{NN\pi}(\bar{N}\boldsymbol{\tau}N)\cdot\boldsymbol{\pi} - if_{\Sigma\Sigma\pi}(\bar{\boldsymbol{\Sigma}}\times\boldsymbol{\Sigma})\cdot\boldsymbol{\pi} \\ & + f_{\Lambda\Sigma\pi}(\bar{\Lambda}\boldsymbol{\Sigma} + \bar{\boldsymbol{\Sigma}}\Lambda)\cdot\boldsymbol{\pi} + f_{\Xi\Xi\pi}(\bar{\Xi}\boldsymbol{\tau}\Xi)\cdot\boldsymbol{\pi} \\ & + f_{\Lambda NK}[(\bar{N}K)\Lambda + \bar{\Lambda}(K^\dagger N)] \\ & + f_{\Xi\Lambda K}[(\bar{\Xi}K_c)\Lambda + \bar{\Lambda}(K_c^\dagger\Xi)] \\ & + f_{\Sigma NK}[\bar{\boldsymbol{\Sigma}}\cdot(K^\dagger\boldsymbol{\tau}N) + (\bar{N}\boldsymbol{\tau}K)\cdot\boldsymbol{\Sigma}] \\ & + f_{\Sigma\Xi K}[\bar{\boldsymbol{\Sigma}}\cdot(K_c^\dagger\boldsymbol{\tau}\Xi) + (\bar{\Xi}\boldsymbol{\tau}K_c)\cdot\boldsymbol{\Sigma}] \\ & + f_{NN\eta_8}(\bar{N}N)\eta_8 + f_{\Lambda\Lambda\eta_8}(\bar{\Lambda}\Lambda)\eta_8 \\ & + f_{\Sigma\Sigma\eta_8}(\bar{\boldsymbol{\Sigma}}\cdot\boldsymbol{\Sigma})\eta_8 + f_{\Xi\Xi\eta_8}(\bar{\Xi}\Xi)\eta_8, \end{aligned} \tag{2.7}$$

for the singlet and octet coupling, respectively, and $f_{NN\pi} = f_8$ and $f_{NN\eta_1} = f_{\Lambda\Lambda\eta_1} = f_{\Sigma\Sigma\eta_1} = f_{\Xi\Xi\eta_1} = f_1$. We have introduced the isospin doublets

$$N = \begin{pmatrix} p \\ n \end{pmatrix}, \quad \Xi = \begin{pmatrix} \Xi^0 \\ \Xi^- \end{pmatrix}, \quad K = \begin{pmatrix} K^+ \\ K^0 \end{pmatrix}, \quad K_c = \begin{pmatrix} \bar{K}^0 \\ -K^- \end{pmatrix}. \tag{8}$$

The phases have been chosen according to [35], such that the inner product of the isovectors $\boldsymbol{\Sigma}$ and $\boldsymbol{\pi}$ is

$$\boldsymbol{\Sigma} \cdot \boldsymbol{\pi} = \Sigma^+\pi^- + \Sigma^0\pi^0 + \Sigma^-\pi^+. \tag{9}$$

The interaction Hamiltonians in Eq. (2.7) are invariant under $\mathrm{SU}_f(3)$ transformations if the coupling constants are expressed in terms of the octet coupling $f_8 \equiv f$ and α as [35]

$$\begin{aligned}
f_{NN\pi} &= f, & f_{NN\eta_8} &= \tfrac{1}{\sqrt{3}}(4\alpha - 1)f, \\
f_{\Xi\Xi\pi} &= -(1 - 2\alpha)f, & f_{\Xi\Xi\eta_8} &= -\tfrac{1}{\sqrt{3}}(1 + 2\alpha)f, \\
f_{\Lambda\Sigma\pi} &= \tfrac{2}{\sqrt{3}}(1 - \alpha)f, & f_{\Sigma\Sigma\eta_8} &= \tfrac{2}{\sqrt{3}}(1 - \alpha)f, \\
f_{\Sigma\Sigma\pi} &= 2\alpha f, & f_{\Lambda\Lambda\eta_8} &= -\tfrac{2}{\sqrt{3}}(1 - \alpha)f, \\
f_{\Lambda NK} &= -\tfrac{1}{\sqrt{3}}(1 + 2\alpha)f, & f_{\Xi\Lambda K} &= \tfrac{1}{\sqrt{3}}(4\alpha - 1)f, \\
f_{\Sigma NK} &= (1 - 2\alpha)f, & f_{\Xi\Sigma K} &= -f,
\end{aligned} \tag{10}$$

and the singlet coupling f_1 as

$$f_{NN\eta_1} = f_{\Lambda\Lambda\eta_1} = f_{\Sigma\Sigma\eta_1} = f_{\Xi\Xi\eta_1} = f_1. \tag{11}$$

The baryon-baryon-meson vertices are thus characterized by only four parameters if $\mathrm{SU}_f(3)$ symmetry is assumed: the octet coupling constant f_8, the singlet coupling constant f_1, the $F/(F + D)$ ratio α, and the mixing angle θ, which gives the relation between the physical and octet and singlet isoscalar mesons. The $\mathrm{SU}_f(3)$ invariant local interaction densities we use for the triple-meson (MMM) vertices are given below.

(i) $J^{PC} = 1^{--}$ *vector mesons*:

$$\begin{aligned}
\mathcal{H}_{PPV} &= g_{PPV} f_{abc} V_\mu^a P^b \overset{\leftrightarrow}{\partial}{}^\mu P^c \\
&= -i\sqrt{2} g_{PPV} \mathrm{Tr} \mathcal{P}_8 \left(\partial_\mu \mathcal{P}_8 \cdot \mathcal{V}_8^\mu - \mathcal{V}_8^\mu \partial_\mu \mathcal{P}_8 \right) \\
&= g_{PPV} [\boldsymbol{\rho}_\mu \cdot (\boldsymbol{\pi} \times \overset{\leftrightarrow}{\partial}{}^\mu \boldsymbol{\pi} + i K^\dagger \boldsymbol{\tau} \overset{\leftrightarrow}{\partial}{}^\mu K) \\
&\quad + (i K_\mu^{*\dagger} \boldsymbol{\tau} K \cdot \overset{\leftrightarrow}{\partial}{}^\mu \boldsymbol{\pi} + \text{h.c.}) \\
&\quad + \sqrt{3}(i K_\mu^{*\dagger} K \overset{\leftrightarrow}{\partial}{}^\mu \eta + \text{h.c.}) \\
&\quad + \sqrt{3} i \phi_{8,\mu} K^\dagger \overset{\leftrightarrow}{\partial}{}^\mu K],
\end{aligned} \tag{2.12}$$

where h.c. stands for the Hermitian conjugate of the preceding term, and we use the usual notation for the derivative $\overset{\leftrightarrow}{\partial}{}^\mu$ acting on the pseudoscalar mesons, $P^b \overset{\leftrightarrow}{\partial}{}^\mu P^c \equiv P^b(\partial^\mu P^c) - (\partial^\mu P^b) \cdot P^c$. The coupling of the vector mesons to the pseudoscalar mesons is $\mathrm{SU}_f(3)$ antisymmetric; the symmetric coupling can be excluded by invoking a generalized Bose symmetry for the pseudoscalar mesons; interchanging the two pseudoscalar mesons leaves $\mathcal{H}_{PPV}$ invariant. The coupling constant for the decay of a ρ meson into two pions is defined as $g_{\pi\pi\rho} = 2\, g_{PPV}$, which can be estimated using the decay width of the ρ meson, see Eq. (4.9).

(ii) $J^{PC} = 0^{++}$ *scalar mesons*:

$$\begin{aligned}
\mathcal{H}_{PPS} &= \frac{\sqrt{3}}{2} g_{PPS} d_{abc} S^a P^b P^c \\
&= \frac{\sqrt{3}}{2\sqrt{2}} g_{PPS} \mathrm{Tr} \mathcal{P}_8 (\mathcal{P}_8 \cdot \mathcal{S}_8 + \mathcal{S}_8 \cdot \mathcal{P}_8) \\
&= g_{PPS} \left[\boldsymbol{a}_0 \cdot \left(\boldsymbol{\pi} \eta + \frac{\sqrt{3}}{2} K^\dagger \boldsymbol{\tau} K \right) \right. \\
&\quad + \frac{\sqrt{3}}{2} (K_0^\dagger \boldsymbol{\tau} K \cdot \boldsymbol{\pi} + \text{h.c.}) - \frac{1}{2} (K_0^\dagger K \eta + \text{h.c.}) \\
&\quad \left. + \frac{1}{2} f_0 (\boldsymbol{\pi} \cdot \boldsymbol{\pi} - K^\dagger K - \eta\eta) \right].
\end{aligned} \tag{2.13}$$

For the scalar mesons, we have a symmetric coupling. The dimensionless coupling constant for the decay of the σ meson into two pions is defined as $g_{\pi\pi\sigma} = g_{PPS}/m_{\pi^+}$, which can be estimated using the decay width of the σ meson, see Eq. (4.9).

(iii) $J^{PC} = 2^{++}$ *tensor-mesons*:

$$\begin{aligned}
\mathcal{H}_{PPT} &= \frac{2 g_{PPT}}{m_{\pi^+}} \left[\boldsymbol{a}_2^{\mu\nu} \cdot \left(\partial_\mu \boldsymbol{\pi} \partial_\nu \eta + \frac{\sqrt{3}}{2} \partial_\mu K^\dagger \boldsymbol{\tau} \partial_\nu K \right) \right. \\
&\quad + \frac{\sqrt{3}}{2} \left(K_2^{\mu\nu\dagger} \boldsymbol{\tau} \partial_\mu K \cdot \partial_\nu \boldsymbol{\pi} + \text{h.c.} \right) \\
&\quad - \frac{1}{2} \left(K_2^{\mu\nu\dagger} \partial_\mu K \partial_\nu \eta + \text{h.c.} \right) \\
&\quad \left. + \frac{1}{2} f_2^{\mu\nu} (\partial_\mu \boldsymbol{\pi} \cdot \partial_\nu \boldsymbol{\pi} - \partial_\mu K^\dagger \partial_\nu K - \partial_\mu \eta \partial_\nu \eta) \right].
\end{aligned} \tag{2.14}$$

The coupling constant for the decay of the f_2 meson into two pions is given by $g_{\pi\pi f_2} = g_{PPT}$, which is estimated in Eq. (4.9).

Some numerical values for the previous coupling constants are given by Nagels *et al.* [36]. The isospin factors resulting from the previous interactions are discussed in Appendix A and listed in Tables I and VII for πN and K^+N interactions, respectively. We note that in the NSC model the $\mathrm{SU}_f(3)$ symmetry is broken dynamically, since we use the physical masses for the baryons and mesons. The $\mathrm{SU}_f(3)$ symmetry for the coupling constants is not necessarily exact; in fact, we allow for a breaking in the NSC K^+N model (see Sec. V).

III. RENORMALIZATION

The Lagrangians used are effective Lagrangians, expressed in terms of the physical coupling constants and masses. Then, in principle, counterterms should be added to the Lagrangian and fixed by renormalization conditions. This is particularly true in channels where bound states and resonances occur. An example is the famous Δ resonance at $M_\Delta = 1232$ MeV in the πN system. The Δ pole diagram gets "dressed" when it

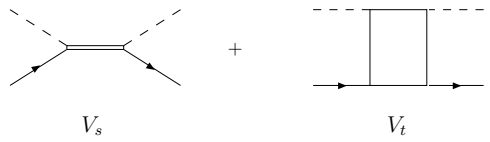

FIG. 1. Pole potential V_s contains s-channel diagrams; nonpole potential V_t contains t- and u-channel diagrams.

is iterated with other graphs upon insertion into an integral equation. Also, it appears that by using only u- and t-channel forces it is impossible to describe the experimental πN phases above resonance in the P_{33} wave. From the viewpoint of the quark model, this is natural, because here the Δ resonance is, at least partly, a genuine three-quark state and should not be described as a pure πN resonance, but it should be treated the same as the nucleons. We take the same attitude toward the other meson-baryon resonances as the Roper, $S_{11}(1535)$, etc. The resonance diagrams split nicely into a pole part having a $(\sqrt{s} - M_0 + i\epsilon)^{-1}$ factor, and a nonpole part having a $(\sqrt{s} + M_0 - i\epsilon)^{-1}$ factor. Here, M_0 is the so-called bare mass. The pole position will move to $\sqrt{s} = M_R$, where M_R is the physical mass of the resonance. This determines the bare mass M_0.

To implement these ideas, we follow Haymaker [37]. We write the total potential V as a sum of a potential containing poles and a potential not containing poles $V(\mathbf{p}', \mathbf{p}) = V_s(\mathbf{p}', \mathbf{p}) + V_t(\mathbf{p}', \mathbf{p})$[1], (see Fig. 1), where

$$V_s(\mathbf{p}', \mathbf{p}) = \sum_i \Gamma_i(\mathbf{p}')\Delta_i(P)\Gamma_i(\mathbf{p}) \tag{3.1}$$

is the pole part of the s-channel baryon exchanges. In Eq. (3.1) the right-hand side is written in terms of the so-called bare couplings and masses. We have $\Delta_i(P) = (\sqrt{s} - M_0 + i\epsilon)^{-1}$, where in the c.m. system $P = (\sqrt{s}, \mathbf{0})$. The other part and the t- and u-channel exchanges are contained in $V_t(\mathbf{p}', \mathbf{p})$. In the following, we treat explicitly the cases when there is only one s-channel bound state or resonance present. It is easy to generalize this to the case with more s-channel poles. Following [37] we define two T matrices T_j, $j = 1, 2$ by

$$T_j = V_j + V_j G T, \qquad T = T_1 + T_2, \tag{3.2}$$

where $V_1 = V_s$ and $V_2 = V_t$. The amplitude T_j is the sum of all graphs in the iteration of T in which the potential V_j "acts last." Defining T_t as the T matrix for the V_t interaction alone, i.e.,

$$T_t = V_t + V_t G T_t, \tag{3.3}$$

it is shown in [37] that

$$T_1 = T_t + T_t G T_2, \qquad T_2 = T_s + T_s G T_t, \tag{3.4}$$

with

$$T_s = V_s + V_s H_1 T_s, \qquad H_1 = G + G T_t G. \tag{3.5}$$

Taking these results together one obtains for the total T matrix the expression

$$T = T_t + T_s + T_t G T_s + T_s G T_t + T_t G T_s G T_t. \tag{3.6}$$

[1]Notice that in Ref. [37] the V and T matrices differ by a $(-)$-sign from those used here.

Since V_s is a separable potential, the solution for T_s in the case of one pole can be written as

$$T_s(\mathbf{p}', \mathbf{p}) = \frac{\Gamma(\mathbf{p}')\Gamma(\mathbf{p})}{\Delta(P)^{-1} - \Sigma(P)} \equiv \Gamma(\mathbf{p}')\Delta^*(P)\Gamma(\mathbf{p}), \tag{3.7}$$

where we introduced the shorthand $\Delta = \Delta_i$, and defined the self-energy Σ and the dressed propagator Δ^* by

$$\begin{aligned} \Sigma(P) &= \int \widetilde{dq'} \int \widetilde{dq''} \Gamma(\mathbf{q}') H_1(\mathbf{q}', \mathbf{q}''; P) \Gamma(\mathbf{q}''), \\ \Delta^*(P) &= \frac{\Delta(P)}{1 - \Delta(P)\Sigma(P)} \\ &= \Delta(P) + \Delta(P)\Sigma(P)\Delta^*(P), \end{aligned} \tag{3.8}$$

where $\widetilde{dq'} = d^3q'/(2\pi)^3$, etc. Inserting Eqs. (3.7) and (3.8) into Eq. (3.6), and exploiting time reversal and parity invariance, which gives $T_t(\mathbf{p}', \mathbf{p}) = T_t(\mathbf{p}, \mathbf{p}')$, one finds the expressions for the total amplitude, dressed vertex, and self-energy to be

$$T(\mathbf{p}', \mathbf{p}) = T_t(\mathbf{p}', \mathbf{p}) + \Gamma^*(\mathbf{p}')\Delta^*(P)\Gamma^*(\mathbf{p}), \tag{3.9}$$

$$\Gamma^*(\mathbf{p}) = \Gamma(\mathbf{p}) + \int \widetilde{dq} \Gamma(\mathbf{q}) G(\mathbf{q}, P) T_t(\mathbf{q}, \mathbf{p}), \tag{3.10}$$

$$\Sigma(P) = \int \widetilde{dq} \Gamma(\mathbf{q}) G(\mathbf{q}, P) \Gamma^*(\mathbf{q}), \tag{3.11}$$

where the dressed propagator $\Delta^*(P)$ is given by

$$\Delta^*(P)^{-1} = \Delta(P)^{-1} - \Sigma(P). \tag{3.12}$$

The equations above show that the complete T matrix can be computed in a straightforward manner, using the full-off-shell T matrix $T_t(\mathbf{p}', \mathbf{p})$, defined in Eq. (3.3). The renormalized pole position $\sqrt{s} = M_R$ is determined by the condition

$$\begin{aligned} 0 &= \Delta^*(\sqrt{s} = M_R)^{-1} \\ &= \Delta(\sqrt{s} = M_R)^{-1} - \Sigma(\sqrt{s} = M_R). \end{aligned} \tag{3.13}$$

A diagrammatic representation of the previous derived equations for the meson-baryon amplitude, potential, dressed vertex, and dressed propagator is given in Fig. 2.

A. Partial wave analysis

The partial wave expansion for vertex function Γ reads

$$\Gamma(\mathbf{p}) = \sqrt{4\pi} \sum_{L,M} \Gamma_L(p) Y_M^L(\hat{\mathbf{p}}), \tag{3.14}$$

and similarly for Γ^*. The partial wave expansion for amplitude T reads

$$T(\mathbf{q}, \mathbf{p}) = 4\pi \sum_{L,M} T_L(q, p) Y_M^L(\hat{\mathbf{q}})^* Y_M^L(\hat{\mathbf{p}}). \tag{3.15}$$

Then, the partial wave projection of the integrals in Eqs. (3.10) and (3.11) become

$$\begin{aligned} \Gamma_L^*(p) &= \Gamma_L(p) + \frac{1}{2\pi^2} \int q^2 dq \Gamma_L(q) G(q, P) T_{t,L}(q, p), \\ \Sigma_L(P) &= \frac{1}{2\pi^2} \int q^2 dq \Gamma_L(q) G(q, P) \Gamma_L^*(q). \end{aligned} \tag{3.16}$$

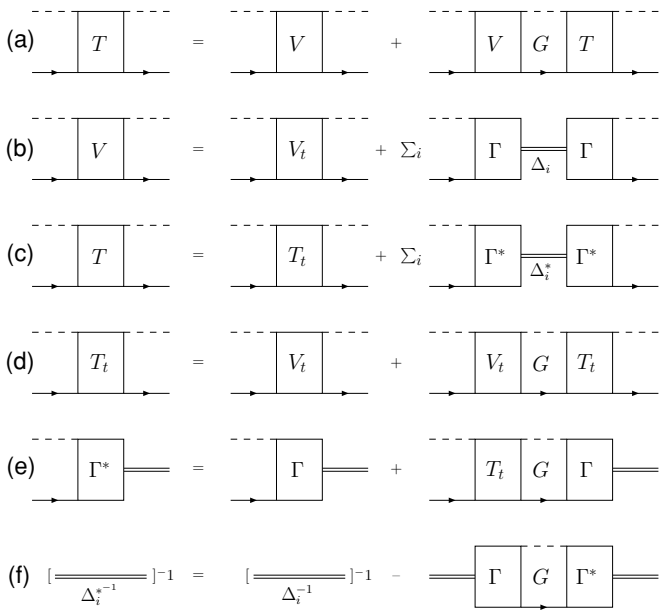

FIG. 2. Integral equation for amplitude in the case of a nonpole and pole potential. (a) Integral equation for the total amplitude. (b) Potential in terms of the nonpole and pole potential. (c) Amplitude in terms of the nonpole and pole amplitude Eq. (3.9). (d) Integral equation for the nonpole amplitude Eq. (3.3). (e) Equation for the dressed vertex Eq. (3.10). (f) Equation for the dressed propagator Eqs. (3.12) and (3.11).

In the following subsections it is understood that we deal with the partial wave quantities. We suppress the angular momenta labels for notational convenience.

B. Multiplicative renormalization parameters

We consider the second part on the right-hand side of Eq. (3.9) to be given in terms of the bare resonance mass M_0 and the bare resonance coupling g_0. We consider only the wave function and vertex renormalization for the resonance, and use the multiplicative renormalization method. Then, since the total Lagrangian is unchanged and Hermitian, unitarity is preserved. The Z transformation for the resonance field reads $\Psi_{0,\mu} = \sqrt{Z_2}\Psi_{r,\mu}$, and for the resonance coupling $g_0 = Z_g g_r$, where the subscripts r and 0 refer to, respectively, the "renormalized" and "bare" field. Applied to the $\Delta N\pi$ interaction, this gives

$$\mathcal{L}_I \sim g_0 \bar{\Psi}_{0,\mu}\psi\partial^\mu\phi = Z_g\sqrt{Z_2}\, g_r \bar{\Psi}_{r,\mu}\psi\partial^\mu\phi, \quad (3.17)$$

where $g_r = f_{\Delta N\pi}/m_{\pi^+}$ is the renormalized, i.e., the physical, and g_0 the unrenormalized, i.e., the bare coupling. Introducing the renormalization constant $Z_1 = Z_g\sqrt{Z_2}$, we have

$$\begin{aligned}\mathcal{L}_I &\sim Z_1 g_r \bar{\Psi}_{r,\mu}\psi\partial^\mu\phi \\ &= g_r \bar{\Psi}_{r,\mu}\psi\partial^\mu\phi + (Z_1 - 1) g_r \bar{\Psi}_{r,\mu}\psi\partial^\mu\phi. \quad (3.18)\end{aligned}$$

From the form of Eq. (3.10) it is useful at this stage to distinguish functions with the bare and physical couplings g_0 and g_r. Therefore, we introduce the vertex functions

$$\Gamma^*_{u,r}(p) = \Gamma_{u,r}(p) + \int \widetilde{dq}\, \Gamma_{u,r}(q) G(q) T_t(q, p), \quad (3.19)$$

with the definitions

$$\Gamma_{u,r}(p) = g_{0,r}\bar{\Gamma}(p), \qquad \Gamma^*_{u,r}(p) = g_{0,r}\bar{\Gamma}^*(p), \quad (3.20)$$

implying the relations

$$\begin{aligned}\Gamma_u(p) &= Z_g \Gamma_r(p), \\ \Gamma^*_u(p) &= Z_g \Gamma^*_r(p), \\ \Sigma_u(P) &= Z_g^2 \Sigma_r(P).\end{aligned} \quad (3.21)$$

1. Resonance renormalization

Working out this renormalization scheme for the baryon resonances, we start, in Eq. (3.9) with the second part on the right-hand side as given in terms of the bare resonance mass M_0 and bare resonance coupling g_0. We write this part of the amplitude as

$$T_{\rm res}(p', p) = \Gamma^*_u(p') \frac{1}{\sqrt{s} - M_0 - \Sigma_u(\sqrt{s})} \Gamma^*_u(p). \quad (3.22)$$

Next, we develop the denominator around the renormalized (i.e., the physical) resonance mass M_R and rearrange terms. We get

$$\begin{aligned}T_{\rm res}(p', p) &= \Gamma^*_u(p') \Bigg[\sqrt{s} - M_0 - \Sigma_u(M_R) \\ &\quad - (\sqrt{s} - M_R)\frac{\partial \Sigma_u}{\partial\sqrt{s}} \ldots \Bigg]^{-1} \Gamma^*_u(p) \\ &= \Gamma^*_u(p') \Bigg[(\sqrt{s} - M_R) \\ &\quad - (\sqrt{s} - M_R)\frac{\partial \Sigma_u}{\partial\sqrt{s}} \ldots \Bigg]^{-1} \Gamma^*_u(p) \\ &= \Gamma^*_u(p') Z_2 \Gamma^*_u(p) \Bigg[(\sqrt{s} - M_R) \\ &\quad - \frac{1}{2}(\sqrt{s} - M_R)^2 Z_2 \frac{\partial^2 \Sigma_u}{(\partial\sqrt{s})^2} \ldots \Bigg]^{-1}.\end{aligned} \quad (3.23)$$

Here, we have introduced the renormalization constant Z_2 defined by

$$\begin{aligned}Z_2 &\equiv \left(1 - \frac{\partial \Sigma_u}{\partial\sqrt{s}}\bigg|_{\sqrt{s}=M_R} \right)^{-1} \\ &= \left(1 - Z_g^2 \frac{\partial \Sigma_r}{\partial\sqrt{s}} \right)^{-1} = 1 + Z_1^2 \frac{\partial \Sigma_r}{\partial\sqrt{s}}. \quad (3.24)\end{aligned}$$

The derivatives in Eq. (3.23) with respect to $\sqrt{s}$ are evaluated at the point $\sqrt{s} = M_R$, as indicated in Eq. (3.24).

Now we require that the residue at the resonance pole be given in terms of the physical coupling, i.e., g_r. In terms of the

renormalized quantities, the amplitude $T_{\rm res}$ of Eq. (3.22) reads

$$T_{\rm res}(p', p) = \Gamma^*_{\rm ren}(p') \frac{1}{\sqrt{s} - M_R - \Sigma^{(2)}_{\rm ren}(\sqrt{s})} \Gamma^*_{\rm ren}(p). \quad (3.25)$$

Here we have defined the renormalized self-energy and the renormalized dressed vertex as

$$\Sigma^{(2)}_{\rm ren}(\sqrt{s}) \equiv Z_2 \Sigma^{(2)}_u(\sqrt{s}), \qquad \Gamma^*_{\rm ren}(p) \equiv \sqrt{Z_2}\Gamma^*_u(p). \quad (3.26)$$

The renormalized self-energy in the last expression in Eq. (3.23) and its first derivative are defined to be zero at the resonance position $\sqrt{s} = M_R$ and is given by

$$\begin{aligned}\Sigma^{(2)}_{\rm ren}(\sqrt{s}) &\equiv \frac{1}{2}(\sqrt{s} - M_R)^2 \left.\frac{\partial^2 \Sigma_{\rm ren}}{(\partial\sqrt{s})^2}\right|_{\sqrt{s}=M_R} + \cdots \\ &= \Sigma_{\rm ren}(\sqrt{s}) - \Sigma_{\rm ren}(M_R) \\ &\quad -(\sqrt{s} - M_R) \left.\frac{\partial \Sigma_{\rm ren}}{\partial\sqrt{s}}\right|_{\sqrt{s}=M_R}. \end{aligned} \quad (3.27)$$

We notice that the imaginary part of the self-energy is not changed by the wave function renormalization. It is straightforward to include $\Im\Sigma(\sqrt{s})$ in the resonance mass M_R as well as in $\Sigma_{\rm ren}(\sqrt{s})$.

The computation of the amplitude $T_{\rm res}(p', p)$, Eq. (3.25), using only renormalized quantities runs as follows. From Eqs. (3.21) and (3.26) and the definition $Z_1 = Z_g\sqrt{Z_2}$, the renormalized vertex is given by

$$\Gamma^*_{\rm ren}(p) = Z_1 \Gamma^*_r(p). \quad (3.28)$$

Notice that $\Gamma^*_r(p_R) = |\Gamma^*_r(p_R)| \exp(i\varphi^*_r(p_R))$, and that this phase can be ignored when defining the effective decay Lagrangian in Eq. (3.18). The renormalization condition for the vertex is that at the pole position ($\sqrt{s} = M_R$) the renormalized vertex is given in terms of the physical coupling constant

$$|\Gamma^*_{\rm ren}(p = p_R)| = Z_1 |g_r \bar{\Gamma}^*(p = p_R)| = g_r \frac{p_R}{\sqrt{3}} \sqrt{E_R + M}, \quad (3.29)$$

which determines Z_1 and, by Eq. (3.24), Z_2 and Z_g. Now the renormalized self-energy and the renormalized dressed vertex are known from Eq. (3.26). In passing we note that the coupling $g_r = f_{\Delta N\pi}/m_\pi$, and the other factors in the second expression of Eq. (3.29) are specific for a P_{33}-wave resonance.

As is clear from this section, one can either express all quantities in terms of the bare parameters (M_0, g_0) or in terms of the renormalized parameters (M_R, g_r).

For the second part of this statement we now express the bare quantities in terms of the renormalized ones. From Eqs. (3.24) and (3.29) we know Z_g, thus

$$g_0^2 = Z_g^2 g_r^2. \quad (3.30)$$

In the following, we denote the real part of the resonance mass by M_R. Also, we want to renormalize at a point that is experimentally accessible. Therefore, we choose for the renormalization point the real part of the resonance position, $\sqrt{s} = M_R$. So actually we consider the real part of the self-energy $\Re\Sigma$ in the previous derivations, and from Eq. (3.23) we have

$$M_R = M_0 + g_0^2 \Re\bar{\Sigma}(M_R), \quad (3.31)$$

giving the bare mass in terms of the renormalized quantities

$$M_0 = M_R - Z_g^2 g_r^2 \Re\bar{\Sigma}(M_R). \quad (3.32)$$

This concludes the demonstration that one may start with the physical parameters and compute the bare parameters (g_0, M_0). Of course, in exploiting M_0 in order to force the pole position at the chosen $\sqrt{s} = M_R$ to be reasonable one must have $M_0 > 0$.

2. Nucleon pole renormalization

The renormalization of the nucleon pole is completely analogous to the resonance renormalization, except for the renormalization point, which is now the nucleon mass and thus below the πN threshold. Here Green's function has no pole and is real. This implies that $\Re\Sigma(M_N) = \Sigma(M_N)$, in contrast to the resonance case. All quantities in the expression for the self-energy, Eq. (3.11), are real at the nucleon pole.

The renormalization condition for the vertex, analogous to Eq. (3.29), is that at the nucleon pole position ($\sqrt{s} = M_N$) the renormalized vertex is given in terms of the physical coupling constant

$$\begin{aligned}|\Gamma^*_{\rm ren}(p = ip_N)| &= Z_1 |g_r \bar{\Gamma}^*(p = ip_N)| \\ &= \left| \frac{f_r}{m_\pi} \frac{\sqrt{3}\, i\ p_N}{\sqrt{E_N + M}} (\sqrt{s} + M) \right|, \end{aligned} \quad (3.33)$$

in the case of pv coupling. This determines the renormalization constant Z_1. In passing we note that the factor in the second expression of Eq. (3.33) is specific for a P_{11}-wave nucleon pole. Since the nucleon pole position lies below the πN threshold, $\Gamma^*(ip_N)$ and in Eq. (3.10) $\Gamma(ip_N)$ and $T_t(q, ip_N)$ are imaginary.

C. Generalization to the multipole case

In case of multiple pole contributions we have the generalized expression for the pole potential Eq. (3.1)

$$V_s(\mathbf{p}', \mathbf{p}) = \sum_i \Gamma_i(\mathbf{p}') \Delta_i(P) \Gamma_i(\mathbf{p}). \quad (3.34)$$

Introducing the auxiliary function $A_i(\mathbf{p})$, one finds from Eq. (3.5), using Eq. (3.34), that the pole amplitude T_s can be written as

$$T_s(\mathbf{p}', \mathbf{p}) = \sum_i \Gamma_i(\mathbf{p}') \Delta_i(P) A_i(\mathbf{p}). \quad (3.35)$$

Substituting this again in Eq. (3.5) one finds that $A_i(\mathbf{p})$ satisfies

$$\begin{aligned}\Gamma_i(\mathbf{p}) = \Bigg[&\Delta_i^{-1}(P)\delta_{ij} - \iint \Gamma_i(\mathbf{p}'') \\ &\times H_1(\mathbf{p}'', \mathbf{p}'; P) \Gamma_j(\mathbf{p}') \Bigg] \Delta_j(P) A_j(\mathbf{p}), \end{aligned} \quad (3.36)$$

which can be solved for $A_j(\mathbf{p})$, and leads to the separable T_s matrix

$$T_s(\mathbf{p}', \mathbf{p}) = \sum_{ij} \Gamma_i(\mathbf{p}') \Bigg[\Delta^{-1}(P) - \int\int \Gamma(\mathbf{p}'') \times H_1(\mathbf{p}'', \mathbf{p}'; P)\Gamma(\mathbf{p}') \Bigg]^{-1}_{ij} \Gamma_j(\mathbf{p}) \equiv \sum_{ij} \Gamma_i(\mathbf{p}') \Big[\Delta^{-1}(P) - \Sigma(P) \Big]^{-1}_{ij} \Gamma_j(\mathbf{p}), \quad (3.37)$$

which obviously is a generalization of Eq. (3.7). In Eq. (3.37) the quantities $\Delta^{-1}(P)$, $\Gamma(\mathbf{p})$, and $H_1(\mathbf{p}'', \mathbf{p}'; P)$ stand for a diagonal matrix, a vector, and a constant in resonance space, respectively. Above, we introduced the generalized self-energy in resonance space as

$$\Sigma_{ij}(P) = \int\int \Gamma_i(\mathbf{p}'') H_1(\mathbf{p}'', \mathbf{p}'; P) \Gamma_j(\mathbf{p}'). \quad (3.38)$$

D. Baryon mixing

In this paragraph we consider the case of two different nucleon states, called N_1 and N_2. Apart from their masses they have identical quantum numbers. In particular, this applies to the ($I = \frac{1}{2}$, $J^P = \frac{1}{2}^+$) states N and the Roper resonance, i.e., the P_{11} wave. Obviously, the resonance space is two dimensional. The bare states N_1 and N_2 will communicate with each other through the transition to the πN states, and will themselves not be eigenstates of the strong Hamiltonian. The eigenstates of the strong Hamiltonian are identified with the physical states N and the Roper, which are mixtures of N_1 and N_2. To perform the renormalization similarly to the case with only one resonance and to define the physical couplings at the physical states, we have to diagonalize the propagator. This can be achieved using a complex orthogonal 2×2 matrix $\mathcal{O}$, $\mathcal{O}\widetilde{\mathcal{O}} = \widetilde{\mathcal{O}}\mathcal{O} = 1$. We can write, similar to Pascalutsa and Tjon [13],

$$\mathcal{O} = \begin{pmatrix} \cos\chi & \sin\chi \\ -\sin\chi & \cos\chi \end{pmatrix}, \quad (3.39)$$

where χ is the complex (N_1, N_2)-mixing angle. Now, since N_1 and N_2 have the same quantum numbers, apart from their couplings and masses, their πN vertices are isomorphic. This implies that the self-energy matrix in Eq. (3.38) can be written as[2]

$$\begin{pmatrix} \Sigma_{11}(P) & \Sigma_{12}(P) \\ \Sigma_{21}(P) & \Sigma_{22}(P) \end{pmatrix}_u = \begin{pmatrix} g^2_{N_1N\pi} & g_{N_1N\pi} g_{N_2N\pi} \\ g_{N_1N\pi} g_{N_2N\pi} & g^2_{N_2N\pi} \end{pmatrix}_u \bar{\Sigma}(P), \quad (3.40)$$

while for the vertices we have

$$\begin{pmatrix} \Gamma_{N_1} \\ \Gamma_{N_2} \end{pmatrix}_u = \begin{pmatrix} g_{N_1N\pi} \\ g_{N_2N\pi} \end{pmatrix}_u \bar{\Gamma}. \quad (3.41)$$

[2]Notice that we distinguish the nucleon in the πN state from that in the $N_{1,2}$ states.

The propagator in Eq. (3.37) is diagonalized by the angle

$$\chi(P) = \frac{1}{2} \arctan \left[2 \left(\frac{g_{N_1N\pi}}{g_{N_2N\pi}} - \frac{g_{N_2N\pi}}{g_{N_1N\pi}} - \frac{M_{N_2} - M_{N_1}}{g_{N_1N\pi} g_{N_2N\pi} \bar{\Sigma}(P)} \right)^{-1}_u \right]. \quad (3.42)$$

We write $\Sigma = \Sigma_u$ in the following for notational convenience. The corresponding eigenvalues are

$$\Delta^*(P)^{-1}(\pm) = \sqrt{s} - \tfrac{1}{2}(M_{0,1} + M_{0,2}) - \Sigma(\pm, P),$$
$$\Sigma(\pm, P) = \big[(\Sigma_{11}(P) + \Sigma_{22}(P)) \pm [(M_{0,2} - M_{0,1} + \Sigma_{22}(P) - \Sigma_{11}(P))^2 + 4\Sigma_{12}(P)^2]^{1/2} \big] / 2. \quad (3.43)$$

Here, we denoted the unrenormalized masses by $M_{0,1} = M_{N_1}$ for the nucleon, and by $M_{0,2} = M_{N_2}$ for the Roper resonance. Likewise, the unrenormalized couplings are denoted as $g_{0,1} \equiv g_{N_1N\pi,u}$ and $g_{0,2} \equiv g_{N_2N\pi,u}$. Then, for example, $\Sigma_{ij}(P) = g_{0,i} g_{0,j} \bar{\Sigma}(P)$. The resonance amplitude $T_{\rm res}$ is a generalization of the second term in Eq. (3.9) and can be rewritten as

$$T_{\rm res}(p', p) = \sum_{ij} \Gamma^*_i(p') \Delta^*_{ij}(P) \Gamma^*_j(p) = \sum_i (\Gamma^*(p')\mathcal{O})_i (\widetilde{\mathcal{O}} \Delta^*(P) \mathcal{O})_{ij} (\widetilde{\mathcal{O}}\Gamma^*(p))_j = \sum_{\alpha=\pm} (\Gamma^*(p')\mathcal{O})_\alpha d^{-1}_\alpha(P) (\widetilde{\mathcal{O}}\Gamma^*(p))_\alpha, \quad (3.44)$$

where the diagonalized propagator is

$$d_\alpha(P) = \sqrt{s} - \tfrac{1}{2}(M_{0,1} + M_{0,2}) - \Sigma(\alpha, P). \quad (3.45)$$

Unlike, the approach taken in Ref. [38], we renormalize the eigenstate $\alpha = (-)$ at the nucleon pole and the eigenstate $\alpha = (+)$ at the Roper resonance position. That is why we formulate the procedure in terms of the bare or unrenormalized parameters and not directly in terms of the physical parameters. This way we can utilize Eqs. (3.40) and (3.41). As we will see, we get four equations from the renormalization conditions on the masses and couplings, with the set of four unknowns $\{M_{0,1}, M_{0,2}, g_{0,1}, g_{0,2}\}$.

For both α solutions, we use $M_0 = (M_{0,1} + M_{0,2})/2$, to obtain the resonance amplitude

$$T_{\rm res}(\alpha) = \Gamma^*_u(\alpha, p') \frac{1}{\sqrt{s} - M_0 - \Sigma(\alpha, \sqrt{s})} \Gamma^*_u(\alpha, p) = \Gamma^*_u(\alpha, p') \Big[\sqrt{s} - M_0 - \Sigma(\alpha, M_R(\alpha)) - (\sqrt{s} - M_R(\alpha)) \frac{\partial \Sigma(\alpha)}{\partial \sqrt{s}} \ldots \Big]^{-1} \Gamma^*_u(\alpha, p) = \Gamma^*_u(\alpha, p') \Big[(\sqrt{s} - M_R(\alpha)) - (\sqrt{s} - M_R(\alpha)) \frac{\partial \Sigma(\alpha)}{\partial \sqrt{s}} \ldots \Big]^{-1} \Gamma^*_u(\alpha, p)$$

$$= \Gamma^*_u(\alpha, p')Z(\alpha)\Gamma^*_u(\alpha, p)\left[(\sqrt{s} - M_R(\alpha)) - \frac{1}{2}(\sqrt{s} - M_R(\alpha))^2 Z(\alpha)\frac{\partial^2\Sigma(\alpha)}{(\partial\sqrt{s})^2}\ldots\right]. \quad (3.46)$$

Here we introduced the renormalization constants $Z(\alpha)$ defined by

$$Z(\alpha) \equiv \left(1 - \frac{\partial\Sigma(\alpha)}{\partial\sqrt{s}}\bigg|_{\sqrt{s}=M_R(\alpha)}\right)^{-1}. \quad (3.47)$$

Also we can define $\Sigma_{\rm ren}(\alpha, \sqrt{s}) \equiv Z(\alpha)\Sigma(\alpha, \sqrt{s})$ similar to Eq. (3.26). Analogously to Eq. (3.27), we introduce the renormalized self-energy by

$$\begin{aligned}\Sigma^{(2)}_{\rm ren}(\alpha, \sqrt{s}) &= \frac{1}{2}(\sqrt{s} - M_R(\alpha))^2\frac{\partial^2\Sigma_{\rm ren}(\alpha)}{(\partial\sqrt{s})^2} + \ldots \\ &= \Sigma_{\rm ren}(\alpha, \sqrt{s}) - \Sigma_{\rm ren}(\alpha, M_R(\alpha)) \\ &\quad - (\sqrt{s} - M_R(\alpha))\frac{\partial\Sigma_{\rm ren}(\alpha)}{\partial\sqrt{s}}, \end{aligned} \quad (3.48)$$

where the derivatives are evaluated at the point $\sqrt{s} = M_R(\alpha)$. The resonance amplitude $T_{\rm res}(\alpha)$ in Eq. (3.46) in terms of the renormalized quantities reads

$$T_{\rm res}(\alpha) = \Gamma^*_{\rm ren}(\alpha, p')\left[\sqrt{s} - M_R(\alpha) - \Sigma^{(2)}_{\rm ren}(\alpha, \sqrt{s})\right]^{-1} \times \Gamma^*_{\rm ren}(\alpha, p), \quad (3.49)$$

where the renormalized vertex is

$$\Gamma^*_{\rm ren}(\alpha, p) \equiv \sqrt{Z(\alpha)}\Gamma^*_u(\alpha, p). \quad (3.50)$$

Starting from Eq. (3.46), we have suppressed the momentum dependence of $T_{\rm res}(\alpha)$ for notational convenience. The renormalization is now performed by application of the following renormalization conditions:

(i) Mass renormalization: The physical masses $M_R(\alpha)$ are given implicitly by

$$M_R(\alpha) = M_0 + \Sigma(\alpha, M_R(\alpha)). \quad (3.51)$$

(ii) Coupling renormalization: The physical coupling constants $g_r(\alpha)$ are given by

$$\begin{aligned}&\left|\lim_{\sqrt{s}\to M_R(\alpha)}(\sqrt{s} - M_R(\alpha))T_{\rm res}(\alpha)\right| \\ &\quad = |\Gamma^*_{\rm ren}(\alpha, p_R)|^2 \\ &\quad = Z(\alpha)|\Gamma^*_u(\alpha, p_R)|^2. \end{aligned} \quad (3.52)$$

Equations (3.51) and (3.52), with $\alpha = \pm$, constitute four equations. These can be solved for the four bare parameters $\{M_{0,1}, M_{0,2}, g_{0,1}, g_{0,2}\}$ using as input the physical masses and coupling constants. We then get

$$\begin{aligned} g_{0,1} &= g_{0,1}[g_r(+), g_r(-); M_R(+), M_R(-)], \\ g_{0,2} &= g_{0,2}[g_r(+), g_r(-); M_R(+), M_R(-)], \\ M_{0,1} &= M_{0,1}[g_r(+), g_r(-); M_R(+), M_R(-)], \\ M_{0,2} &= M_{0,2}[g_r(+), g_r(-); M_R(+), M_R(-)]. \end{aligned} \quad (3.53)$$

From these, we obtain the renormalization constants

$$Z_g(-) \equiv g_{0,1}/g_r(-), \qquad Z_g(+) \equiv g_{0,2}/g_r(+). \quad (3.54)$$

Notice that after the diagonalization of the propagator we have two uncoupled systems $\alpha = \pm$. Therefore, it is natural to define, in analogy with the single resonance case, the $Z_1(\alpha)$ factors by

$$\begin{aligned}\Gamma^*_{\rm ren}(\alpha, p) &= \sqrt{Z_2(\alpha)}\Gamma^*_u(\alpha, p) \\ &\equiv Z_1(\alpha)Z_g^{-1}(\alpha)\Gamma^*_u(\alpha, p) \\ &\equiv Z_1(\alpha)\Gamma^*_r(\alpha, p), \end{aligned} \quad (3.55)$$

where $Z_2(\alpha) \equiv Z(\alpha)$. Rotating back to the basis (N_1, N_2), we find the Z transformation on the original basis before the diagonalization of the propagator. This Z transformation on the unmixed fields is a 2×2 matrix. Note that in Eqs. (3.54) and (3.55), we have defined several Z factors suggestively. In order to find out how these constants are related to the Z matrices alluded to above, we would have to work out this Z transformation in detail. This we do not attempt, since it is not really necessary here.

From the input of the four physical parameters $\{M_R(\alpha), g_r(\alpha)\}$, one computes the bare parameters. Using the latter, one computes $\Sigma_{\rm ren}(\alpha, \sqrt{s})$ and $\Gamma^*_{\rm ren}(\alpha, p)$. This unambiguously defines the resonance part of the amplitudes.

IV. THE πN INTERACTION

A. The NSC πN model

The potential for πN interactions consists of the one-meson-exchange and one-baryon-exchange Feynman diagrams, derived from effective meson-baryon interaction Hamiltonians (see paper I and Sec. II). The diagrams contributing to the πN potential are given in Fig. 3. The partial wave potentials together with the πN Green's function constitute the kernel of the integral equation for the partial wave T matrix which is solved numerically to find the observable quantities or the phase shifts. We solve the partial wave T matrix by matrix inversion, and we use the method introduced by Haftel and Tabakin [39] to deal numerically with singularities in the physical region in the Green's function.

The interaction Hamiltonians from which the Feynman diagrams are derived are explicitly given below for the πN system. We use the pseudovector coupling for the $NN\pi$ vertex

$$\mathcal{H}_{NN\pi} = \frac{f_{NN\pi}}{m_{\pi^+}}(\bar{N}\gamma_5\gamma_\mu\boldsymbol{\tau}N)\cdot\partial^\mu\boldsymbol{\pi}. \quad (4.1)$$

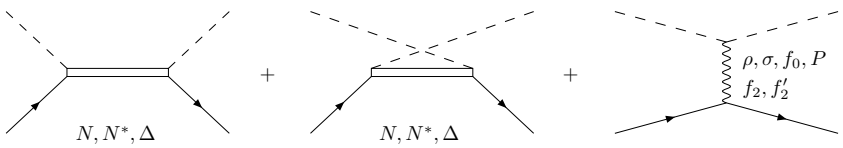

FIG. 3. Contributions to the πN potential from the s-, u- and t-channel Feynman diagrams. The external dashed and solid lines are always the π and N respectively.

The same structure is used for the Roper; and for $S_{11}(1535)$ we use a similar coupling where γ_5 is omitted. The $NN\pi$ coupling constant is determined quite well and is fixed in the fitting procedure. For the $N\Delta\pi$ vertex, we use the conventional coupling

$$\mathcal{H}_{N\Delta\pi} = \frac{f_{N\Delta\pi}}{m_{\pi^+}}(\bar{\Delta}_\mu \boldsymbol{T} N)\cdot\partial^\mu\boldsymbol{\pi} + \text{h.c.}, \tag{4.2}$$

where $\boldsymbol{T}$ is the transition operator between isospin-$\frac{1}{2}$ isospin-$\frac{3}{2}$ states [40]. The only vector meson exchanged in πN scattering is ρ. The $NN\rho$ and $\pi\pi\rho$ couplings we use are

$$\begin{aligned}\mathcal{H}_{NN\rho} &= g_{NN\rho}(\bar{N}\gamma_\mu\boldsymbol{\tau}N)\cdot\boldsymbol{\rho}^\mu \\ &\quad + \frac{f_{NN\rho}}{4\mathcal{M}}(\bar{N}\sigma_{\mu\nu}\boldsymbol{\tau}N)\cdot(\partial^\mu\boldsymbol{\rho}^\nu - \partial^\nu\boldsymbol{\rho}^\mu), \\ \mathcal{H}_{\pi\pi\rho} &= \frac{g_{\pi\pi\rho}}{2}\boldsymbol{\rho}_\mu\cdot\boldsymbol{\pi}\times\overleftrightarrow{\partial}^\mu\boldsymbol{\pi}.\end{aligned} \tag{4.3}$$

We remark that the vector-meson dominance model predicts the ratio of the tensor and vector coupling to be $\kappa_\rho = f_{NN\rho}/g_{NN\rho} = 3.7$, but in πN models it appears to be considerably lower [8,12,13]. We also find a lower value for κ_ρ (see later in Table III). The scalar-meson couplings have the simple structure

$$\mathcal{H}_{NN\sigma} = g_{NN\sigma}\bar{N}N\sigma, \tag{4.4}$$

$$\mathcal{H}_{\pi\pi\sigma} = \frac{g_{\pi\pi\sigma}}{2}m_{\pi^+}\sigma\boldsymbol{\pi}\cdot\boldsymbol{\pi}. \tag{4.5}$$

In contrast with other πN models, our model considers the scalar mesons as genuine $\mathrm{SU}_f(3)$ octet particles. Therefore, not only the σ is exchanged but also the $f_0(975)$ having the same structure for the coupling, both giving an attractive contribution. The contribution of σ exchange is, however, much larger than the contribution of f_0 exchange. A repulsive contribution is obtained from Pomeron exchange, also having the same structure for the coupling. The contributions of the Pomeron and the scalar mesons cancel each other almost completely, as can be seen in the figures for the partial wave potentials (Fig. 4). This cancellation is important in order to comply with the soft-pion theorems for low-energy πN scattering [33,34]. σ and ρ are treated as broad mesons; for details about the treatment, refer to Ref. [41]. σ is considered not as an $\mathrm{SU}_f(3)$ particle in other πN models, but, e.g., as an effective representation of correlated two-pion exchange [10,11,13]; in that case, its contribution may be repulsive in some partial waves.

We consider the exchange of the two isoscalar tensor mesons f_2 and f_2'; the structure of the couplings we use is

$$\begin{aligned}\mathcal{H}_{NNf_2} &= \left[\frac{iF_{1NNf_2}}{4}\bar{N}(\gamma_\mu\overleftrightarrow{\partial}_\nu + \gamma_\nu\overleftrightarrow{\partial}_\mu)N\right. \\ &\quad \left. - \frac{F_{2NNf_2}}{4}\bar{N}\,\overleftrightarrow{\partial}^\mu\overleftrightarrow{\partial}^\nu\,N\right] f_2^{\mu\nu}, \\ \mathcal{H}_{\pi\pi f_2} &= \frac{g_{\pi\pi f_2}}{m_{\pi^+}}f_2^{\mu\nu}(\partial_\mu\boldsymbol{\pi}\cdot\partial_\nu\boldsymbol{\pi}),\end{aligned} \tag{4.6}$$

and the coupling of f_2' is similar to the f_2 coupling. Similar to the case of scalar mesons f_0 and σ, the f_2' contribution is very small compared to the f_2 contribution.

TABLE I. Isospin factors for the various exchanges for a given total isospin I of the πN system.

Exchange	$I = \frac{1}{2}$	$I = \frac{3}{2}$
σ, f_0, f_2, f_2'	1	1
ρ	-2	1
$N(s$ channel)	3	–
$N(u$ channel)	-1	2
$\Delta(s$ channel)	–	1
$\Delta(u$ channel)	$\frac{4}{3}$	$\frac{1}{3}$

The isospin structure results in the isospin factors listed in Table I, see also Appendix A. The spin-space amplitudes in paper I need to be multiplied by these isospin factors to find the complete πN amplitude.

Summarizing, we consider in the t channel the exchanges of the scalar mesons σ, f_0, the Pomeron, the vector meson ρ, and the tensor mesons f_2 and f_2'; and in the u and s channels, the exchanges of the baryons N, Δ, Roper, and S_{11}.

The latter two resonances were included in the NSC πN model to give a good description of the P_{11}- and S_{11}-wave phase shifts at higher energies; their contribution at lower energies is small. These resonances were also included in the model of Pascalutsa and Tjon [13].

It is instructive to examine the relative strength of the contributions of the various exchanges for each partial wave. The on-shell partial wave potentials are given for each partial wave in Figs. 4–6. The pole contributions for the Δ, Roper, and S_{11} are omitted from the P_{33}, P_{11}, and S_{11} waves to show the other contributions more clearly.

We observe that for the s-channel diagrams, only the positive-energy intermediate state develops a pole and is

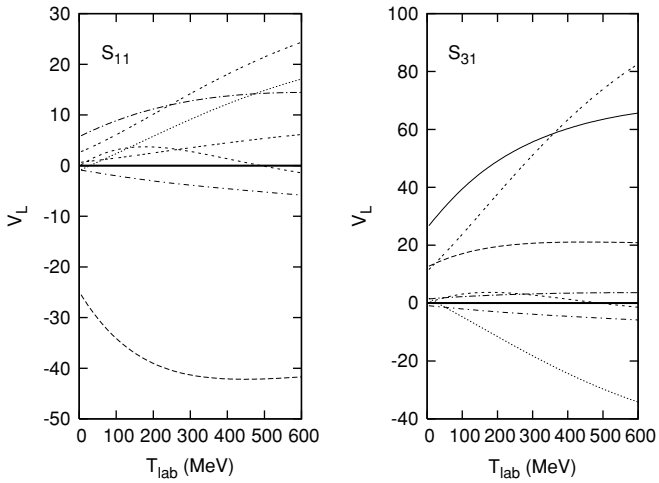

FIG. 4. Total πN S_{11} and S_{31} partial wave potentials V_L as a function of T_{lab} are given by the solid line. For the S_{11} wave, the resonance pole and total contributions are omitted. The various contributions are (a) long dashed line: ρ, (b) short dashed line: Scalar mesons and Pomeron, (c) dotted line: Nucleon exchange, (d) long dash-dotted line: Δ exchange (e) short dash-dotted line: Tensor mesons, (f) double dashed line: Nucleon or Δ pole, and (g) triple dashed line: Roper pole.

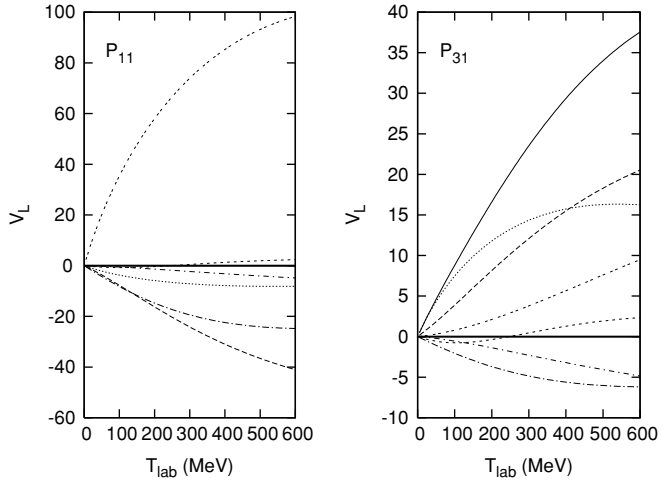

FIG. 5. As in Fig. 4, but for the P_{11} and P_{31} partial wave potentials. For the P_{11} wave, the resonance pole and total contributions are omitted.

nonzero only in the partial wave having the same quantum numbers as the considered particle. The negative-energy intermediate state (background contribution), which is also included in a Feynman diagram, does not have a pole and may contribute to other waves having the same isospin. These background contributions from the nucleon and Δ pole to the S_{11} and S_{31} waves are not small.

The Pomeron-σ cancellation is clearly seen in all partial waves. The nucleon exchange is quite strong in the P waves, except for the P_{11} wave where the nucleon pole is quite strong and gives a repulsive contribution, which causes negative phase shifts at low energies in this wave. The change of sign of the phase shift in the P_{11} wave is caused by the attractive ρ and Δ exchange.

The Δ pole dominates the P_{33} wave, but a large contribution is also present in the S_{31} wave, and a small contribution

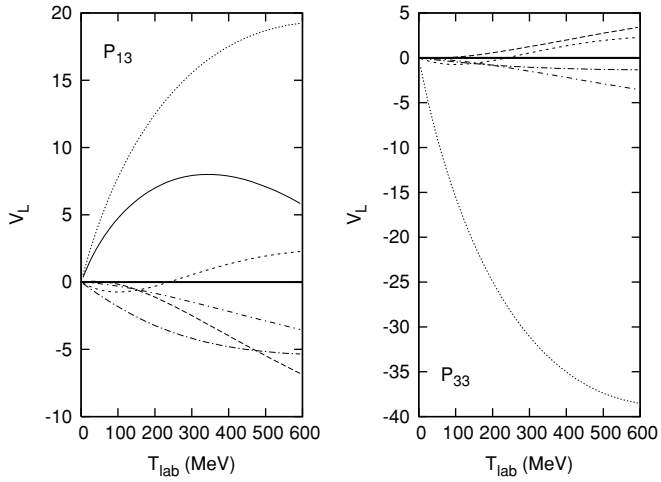

FIG. 6. As in Fig. 4, but for the P_{13} and P_{33} partial wave potentials. For the P_{33} wave, the resonance pole and total contributions are omitted.

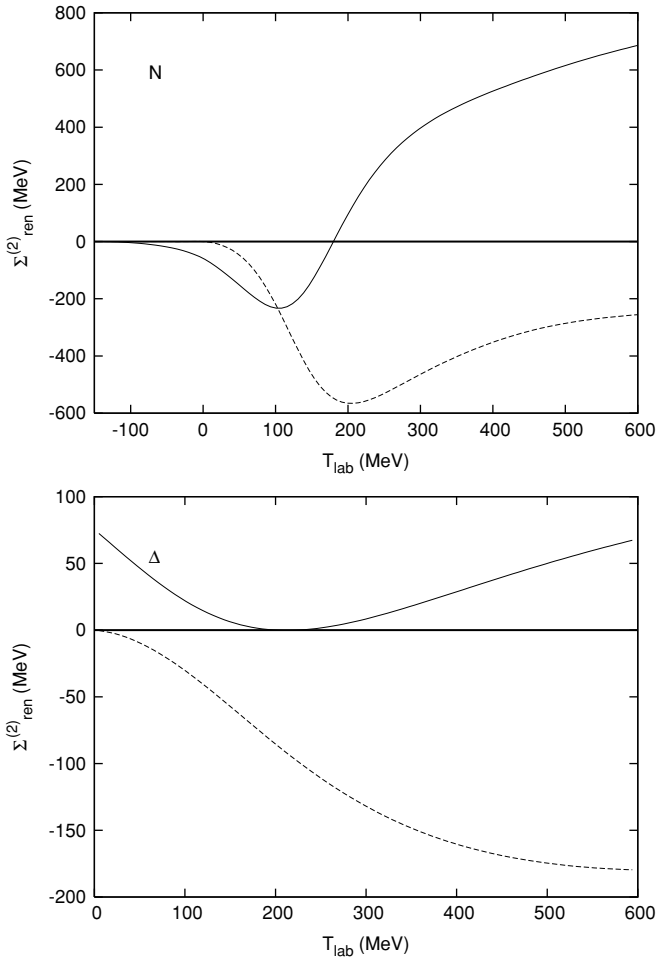

FIG. 7. Renormalized self-energy $\Sigma^{(2)}_{\rm ren}$ of Eqs. (3.48) and (3.27) for the nucleon and the Δ as a function of $T_{\rm lab}$. The real part is given by the solid line; the imaginary part, by the dashed line.

is seen in the P_{31} wave. This contribution results from the spin-1/2 component of the Rarita-Schwinger propagator. The Δ exchange is present in all partial waves. A significant contribution of ρ exchange is seen in all partial waves, except the P_{33} wave, which is dominated by nucleon exchange and, of course, the Δ pole. A modest contribution from the tensor mesons is seen in all partial waves.

When solving the integral equation for the T matrix, the propagator and vertices of the s-channel diagrams get dressed. The renormalization procedure, described in Sec. III, determines the bare masses and coupling constants in terms of the physical parameters. The physical parameters and bare parameters obtained from the fitting procedure are given later in Tables III and IV, respectively. The self-energy of the baryons in the s channel is renormalized, ensuring a pole at the physical mass of the baryons. For the nucleon and the Δ we show the energy dependence of the renormalized self-energy in Fig. 7. This figure clearly shows that the real part of the renormalized self-energy of the Δ and its derivative vanish at the Δ pole, by definition. This is, of course, also the case for the nucleon renormalized self-energy; however, the nucleon pole lies below the πN threshold.

1. Decay coupling constants

The physical coupling constants of the resonances included in the NSC model can be estimated by relating the width of the resonance to the T-matrix element of its decay into two particles, in this case πN. This relation for the two-particle decay is derived in Ref. [42], the two-particle width is

$$\Gamma(p) = \frac{p}{4M^2} \int \frac{d\cos\theta}{4\pi} \sum_{\sigma} |T|^2 , \tag{4.7}$$

where M is the resonance mass and the absolute square of the T matrix is summed over the nucleon spin. The decay processes $\Delta \to \pi N$, $N^* \to \pi N$, and $S_{11} \to \pi N$ are considered in order to find an estimate for the coupling constants $f_{N\Delta\pi}$, $f_{NN^*\pi}$, and $f_{NS_{11}\pi}$, respectively. The T-matrix elements of the various decays in lowest order can be calculated using the interaction Hamiltonians defined in Sec. II and paper I; Eq. (4.7) gives us the estimates for the coupling constants

$$\begin{aligned}
\frac{f^2_{N\Delta\pi}}{4\pi} &= 3\frac{M_\Delta}{E+M}\frac{m^2_{\pi^+}\Gamma}{p^3} \approx 0.39, \\
\frac{f^2_{NN^*\pi}}{4\pi} &= \frac{1}{3}\frac{m^2_{\pi^+}}{(M_{N^*}+M)^2}\frac{(E+M)M_{N^*}\Gamma}{p^3} \approx 0.012, \\
\frac{f^2_{NS_{11}\pi}}{4\pi} &= \frac{1}{3}\frac{m^2_{\pi^+}}{(M_{S_{11}}-M)^2}\frac{M_{S_{11}}}{E+M}\frac{\Gamma}{p} \approx 0.002.
\end{aligned} \tag{4.8}$$

The numerical values are obtained by using the Breit-Wigner masses and widths from the Particle Data Group.

The coupling constants for the decay of the ρ, σ, and f_2 into two pions can be estimated in the same way:

$$\begin{aligned}
\frac{g_{\pi\pi\rho}}{\sqrt{4\pi}} &= \sqrt{\frac{3}{2}m^2_\rho\frac{\Gamma}{p^3}} \approx 1.70, \\
\frac{g_{\pi\pi\sigma}}{\sqrt{4\pi}} &= \sqrt{2\frac{m^2_\sigma}{m^2_{\pi^+}}\frac{\Gamma}{p}} \approx 10.6, \\
\frac{g_{\pi\pi f_2}}{\sqrt{4\pi}} &= \sqrt{\frac{15}{16}m^2_{f_2}m^2_{\pi^+}\frac{\Gamma}{p^5}} \approx 0.224.
\end{aligned} \tag{4.9}$$

B. Results and discussion for πN scattering

We have fitted the NSC πN model to the energy-dependent SM95 partial wave analysis [21] up to pion kinetic laboratory energy $T_{\rm lab} = 600$ MeV. The results are given in Figs. 8 and 9, showing the calculated and empirical phase shift for the SM95 and KH80 [23] phase shift analyses, respectively. The calculated and empirical scattering lengths for the S and P waves are listed in Table II.

A good agreement between the NSC πN model and the empirical phase shifts is found, but at higher energies some deviations are observed in some partial waves. These deviations may be caused by inelasticities, which become important at higher energies and have not been considered in this model. The scattering lengths have been reproduced quite well, except for the $I = \frac{1}{2}$ P waves, for which the NSC πN-model scattering lengths deviate a little from Ref. [21].

First we attempted to generate the Δ resonance dynamically; however, it was not possible to find the correct energy behavior for the P_{33} phase shift. Then we considered the Δ resonance, at least partially, as a three-quark state and included it explicitly in the potential, as done in the modern πN literature, and immediately found the correct energy behavior for the P_{33} phase shift. The other resonances have been treated in the same way.

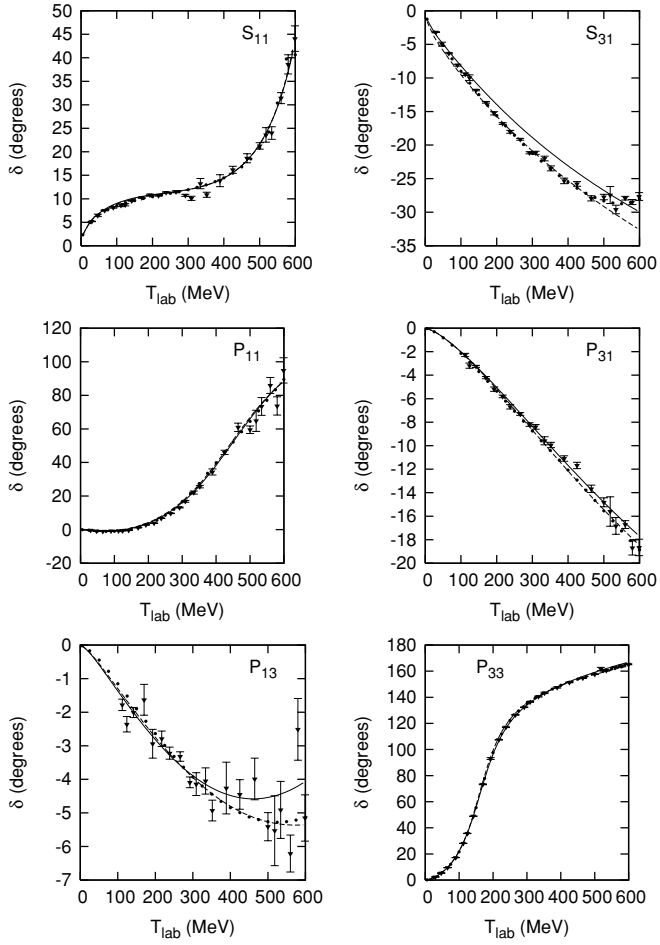

FIG. 8. S- and P-wave πN phase shifts δ as a function of $T_{\rm lab}$. Empirical phases are from SM95 [21], dots are the multienergy phases, and triangles with error bars are the single-energy phases. NSC πN model is given by the solid lines; dashed line is the model without tensor mesons.

We use six different cutoff masses, which are free parameters in the fitting procedure. For the nucleon and the Roper, we use the same cutoff mass; for the two scalar mesons, we use

TABLE II. Calculated and empirical πN S-wave and P-wave scattering lengths in units of m_π^{-1} and m_π^{-3}.

Scat. length	Model	SM95 [21]	KH80 [23]
S_{11}	0.171	0.172	0.173 ± 0.003
S_{31}	−0.096	−0.097	-0.101 ± 0.004
P_{11}	−0.060	−0.068	-0.081 ± 0.002
P_{31}	−0.037	−0.040	-0.045 ± 0.002
P_{13}	−0.031	−0.021	-0.030 ± 0.002
P_{33}	0.213	0.209	0.214 ± 0.002

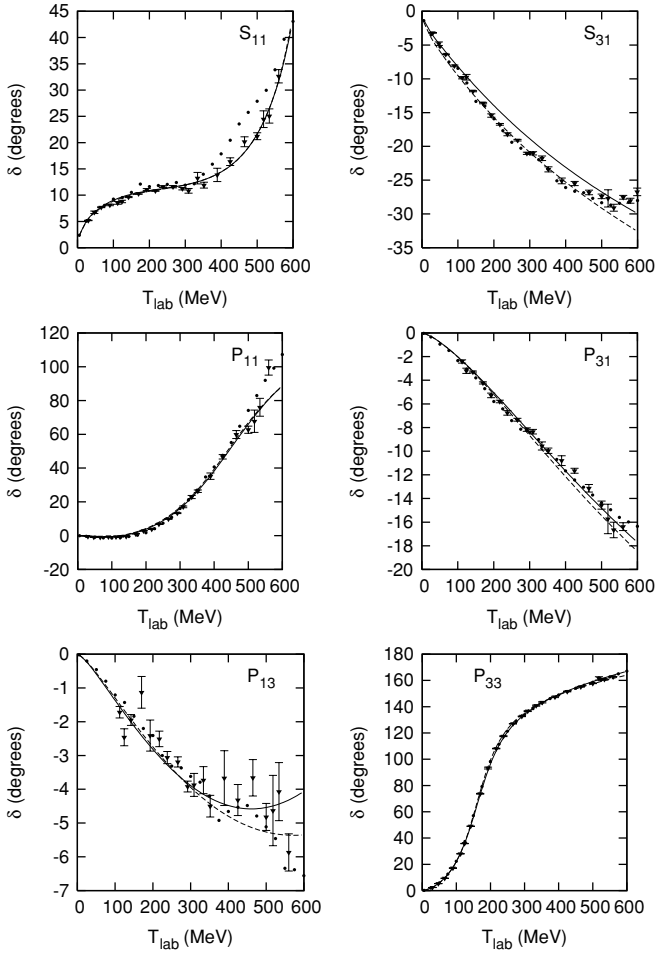

FIG. 9. As in Fig. 8, but with the empirical phases from KH80 [23].

the same cutoff mass; and for the two tensor mesons, the same cutoff mass is used. The masses of the mesons and the nucleon have been fixed in the fitting procedure, but the masses of the resonances are free parameters.

Table III shows that the pole positions of these resonances are not necessarily exactly the same as the resonance positions, because of the nonresonance part of the amplitude, see Eq. (3.9). The Δ and Roper resonate at, respectively, $\sqrt{s} = 1232$ and $\sqrt{s} = 1440$ MeV, while the poles are located at $\sqrt{s} = 1254$ and $\sqrt{s} = 1440$ MeV, respectively.

In order to obtain a good fit, we had to introduce an off-mass-shell damping for the u-channel Δ exchange; we used the factor $\exp[(u - M_\Delta^2)\gamma^2/M_\Delta^2]$, where $\gamma = 1.18$ was a free parameter in the fitting procedure.

Only the product of two coupling constants is determined in the fitting procedure. Therefore, the triple-meson coupling constants are fixed at the value calculated from their decay width, see Subsec. IV A1, and the baryon-baryon-meson coupling constant is a free parameter in the fitting procedure. The resonance coupling constants are first calculated from their decay width, see Subsec. IV A1, but are also treated as free parameters. The fitted and calculated values deviate only a little.

TABLE III. NSC πN-model parameters: coupling constants, masses (MeV), and cutoff masses (MeV). Numbers with an asterisk were fixed in the fitting procedure.

Exch.	Coupling constants		Mass	Λ
ρ	$\frac{g_{NN\rho}g_{\pi\pi\rho}}{4\pi} = 1.333$	$\frac{f_{NN\rho}}{g_{NN\rho}} = 2.121$	770*	838
σ	$\frac{g_{NN\sigma}g_{\pi\pi\sigma}}{4\pi} = 26.196^*$		760*	1126
f_0	$\frac{g_{NNf_0}g_{\pi\pi f_0}}{4\pi} = -1.997^*$		975*	1126
f_2	$\frac{g_{NNf_2}g_{\pi\pi f_2}}{4\pi} = 0.157^*$	$\frac{f_{NNf_2}}{g_{NNf_2}} = 0.382^*$	1270*	412
f_2'	$\frac{g_{NNf_2'}g_{\pi\pi f_2'}}{4\pi} = 0.003^*$	$\frac{f_{NNf_2'}}{g_{NNf_2'}} = 3.393^*$	1525*	412
Pom.	$\frac{g_{NNP}g_{\pi\pi P}}{4\pi} = 4.135$		315	
N	$\frac{f^2_{NN\pi}}{4\pi} = 0.075^*$		938.3*	665
Δ	$\frac{f^2_{N\Delta\pi}}{4\pi} = 0.478$		1254	603
N^*	$\frac{f^2_{NN^*\pi}}{4\pi} = 0.023$		1440	665
S_{11}	$\frac{f^2_{NS_{11}\pi}}{4\pi} = 0.003$		1567	653

The NSC πN model has 17 free physical fit parameters; 3 meson and Pomeron coupling constants, 6 cutoff masses, 4 masses, 3 decay coupling constants, and γ. The values of the coupling constants, listed in Table III, are in good agreement with the literature; $g_{NN\rho} = 0.78$ and $g_{NN\sigma} = 2.47$. However, the tensor coupling constant for ρ, $f_{NN\rho}/g_{NN\rho} = 2.12$, is small compared with values obtained in NN models and the vector dominance value of 3.7. Other πN models [8,13] also suffer from this problem. The $NN\pi$ coupling constant, which is quite well determined in the NN interaction, has been fixed in the NSC πN model. Notice that for the tensor mesons we used the coupling constants $g_T = \mathcal{M}F_1 + \mathcal{M}^2F_2$ and $f_T = -\mathcal{M}^2F_2$ in Table III. Furthermore, the Pomeron cutoff [43] is determined by its "mass" in Table III.

The two conditions in the renormalization procedure for the pole contributions result in the two renormalization constants, i.e., the bare coupling constant and mass, listed in Table IV. We found the bare coupling constants to be smaller than the physical coupling constants except for the S_{11} resonance. The bare masses are larger than the physical masses for each type of exchange; the interaction shifts the bare mass down to the physical mass. Pascalutsa and Tjon [13] find a larger physical mass than bare mass for the Roper. This is probably caused by the choice of the renormalization point. They renormalize

TABLE IV. Renormalization parameters: bare masses (MeV) and coupling constants. Renormalization conditions determine the bare parameters in terms of the model parameters in Table III.

Exch.	Bare coupling constants	Bare mass
N	$\frac{f^2_{0NN\pi}}{4\pi} = 0.013$	1187
Δ	$\frac{f^2_{0N\Delta\pi}}{4\pi} = 0.167$	1399
N^*	$\frac{f^2_{0NN^*\pi}}{4\pi} = 0.015$	1831
S_{11}	$\frac{f^2_{0NS_{11}\pi}}{4\pi} = 0.018$	1774

TABLE V. As in Table III, but without tensor mesons.

Exch.	Coupling constants		Mass	Λ
ρ	$\frac{g_{NN\rho}g_{\pi\pi\rho}}{4\pi} = 1.282$	$\frac{f_{NN\rho}}{g_{NN\rho}} = 1.730$	770*	717
σ	$\frac{g_{NN\sigma}g_{\pi\pi\sigma}}{4\pi} = 26.196$*		760*	864
f_0	$\frac{g_{NNf_0}g_{\pi\pi f_0}}{4\pi} = -1.997$*		975*	864
Pom.	$\frac{g_{NNP}g_{\pi\pi P}}{4\pi} = 4.453$		296	
N	$\frac{f^2_{NN\pi}}{4\pi} = 0.075$*		938.3*	728
Δ	$\frac{f^2_{N\Delta\pi}}{4\pi} = 0.470$		1249	659
N^*	$\frac{f^2_{NN^*\pi}}{4\pi} = 0.021$		1441	728
S_{11}	$\frac{f^2_{NS_{11}\pi}}{4\pi} = 0.003$		1557	482

the Roper contribution at the nucleon pole; we think it is more natural to perform the renormalization at the Roper pole.

Besides the discussed NSC πN model, we also considered a model that does not contain tensor mesons. We fitted this model to the empirical phase shifts, and the results of the fit are given by the dashed lines in Fig. 8 and 9. We notice that in two partial waves, a noticeable difference can be seen between the two models; the S_{11} partial wave is described better by this model than by the NSC πN model. It is hard to say which model works better for the P_{13} partial wave, since the single-energy phase shifts have large error bars and both models are in agreement with the P_{13} phase shifts. The tensor mesons are important for a good description of the K^+N data, as shown in the next section. The πN scattering lengths are approximately the same for both models.

The parameters belonging to this model are listed in Table V, and the bare masses and coupling constants are given in Table VI. The values of the coupling constants are essentially the same for both models, except for $f_{NN\rho}/g_{NN\rho}$. The values of the form factors vary for both models.

Since the S-wave scattering lengths are reproduced well, the soft-pion theorems for low-energy πN scattering [33] are satisfied in the NSC πN model, without the need for a derivative coupling for the $\pi\pi\sigma$ vertex. In view of chiral perturbation theory inspired models, the chiral c_1, c_3, and c_4 terms are described implicitly by the NSC πN model, since this model gives a good description of the empirical phase shifts.

V. THE K^+N INTERACTION

A. The NSC K^+N model

The NSC K^+N model is an $SU_f(3)$ extension of the NSC πN model and consists analogously of the one-meson-exchange and one-baryon-exchange Feynman diagrams. The various diagrams contributing to the K^+N potential are given in Fig. 10. The interaction Hamiltonians from which the Feynman diagrams for the K^+N system are derived are

TABLE VI. As in Table IV, but without tensor mesons.

Exch.	Bare coupling constants	Bare mass
N	$\frac{f^2_{0NN\pi}}{4\pi} = 0.011$	1203
Δ	$\frac{f^2_{0N\Delta\pi}}{4\pi} = 0.159$	1417
N^*	$\frac{f^2_{0NN^*\pi}}{4\pi} = 0.022$	1944
S_{11}	$\frac{f^2_{0NS_{11}\pi}}{4\pi} = 0.016$	1602

explicitly given below. We use the pseudovector coupling for the $N\Lambda K$ and $N\Sigma K$ vertex,

$$\begin{aligned}\mathcal{H}_{N\Lambda K} &= \frac{f_{N\Lambda K}}{m_{\pi^+}}(\bar{N}\gamma_5\gamma_\mu\partial^\mu K)\Lambda + \text{h.c.},\\ \mathcal{H}_{N\Sigma K} &= \frac{f_{N\Sigma K}}{m_{\pi^+}}(\bar{N}\gamma_5\gamma_\mu\boldsymbol{\tau}\partial^\mu K)\cdot\boldsymbol{\Sigma} + \text{h.c.}.\end{aligned} \tag{5.1}$$

The coupling constants are determined by the $NN\pi$ coupling constant, and the $F/(F+D)$ ratio α_P. For $\Lambda(1405)$, we use a similar coupling where γ_5 is omitted. For the $N\Sigma^*K$ vertex we use, just as for the $N\Delta\pi$ vertex, the conventional coupling

$$\mathcal{H}_{N\Sigma^*K} = \frac{f_{N\Sigma^*K}}{m_{\pi^+}}(\bar{N}\boldsymbol{\tau}\partial^\mu K)\cdot\boldsymbol{\Sigma}^*_\mu + \text{h.c.}. \tag{5.2}$$

Since the $SU_f(3)$ decuplet occurs only once in the direct product of two octets, there is no mixing parameter α for this coupling. The $N\Sigma^*K$ coupling is determined by $SU_f(3)$, $f^2_{N\Sigma^*K} = f^2_{N\Delta\pi}/3$. Besides the ρ, the isoscalar vector mesons ω and ϕ are also exchanged. The following vector-meson couplings are used:

$$\begin{aligned}\mathcal{H}_{NN\rho} &= g_{NN\rho}(\bar{N}\gamma_\mu\boldsymbol{\tau}N)\cdot\boldsymbol{\rho}^\mu\\ &\quad + \frac{f_{NN\rho}}{4\mathcal{M}}(\bar{N}\sigma_{\mu\nu}\boldsymbol{\tau}N)\cdot(\partial^\mu\boldsymbol{\rho}^\nu - \partial^\nu\boldsymbol{\rho}^\mu),\\ \mathcal{H}_{NN\omega} &= g_{NN\omega}\bar{N}\gamma_\mu N\omega^\mu\\ &\quad + \frac{f_{NN\omega}}{4\mathcal{M}}\bar{N}\sigma_{\mu\nu}N(\partial^\mu\omega^\nu - \partial^\nu\omega^\mu),\end{aligned} \tag{5.3}$$

$$\begin{aligned}\mathcal{H}_{KK\rho} &= g_{KK\rho}\boldsymbol{\rho}_\mu\cdot(iK^\dagger\boldsymbol{\tau}\overset{\leftrightarrow}{\partial}{}^\mu K),\\ \mathcal{H}_{KK\omega} &= g_{KK\omega}\omega_\mu(iK^\dagger\overset{\leftrightarrow}{\partial}{}^\mu K).\end{aligned} \tag{5.4}$$

The coupling of ϕ is similar to the ω coupling. Although we include ϕ exchange, its contribution is negligible compared to ω exchange. The coupling constants $g_{KK\omega}$ and $g_{KK\phi}$ are fixed by $SU_f(3)$ in terms of $g_{\pi\pi\rho}$ and θ_V. The $NN\omega$ coupling constant is a free parameter, and the $NN\phi$ coupling constant depends on θ_V, α_V, and the other two coupling constants. In addition to σ and f_0 exchange, the isovector scalar meson a_0 is also exchanged. The following scalar-meson couplings are

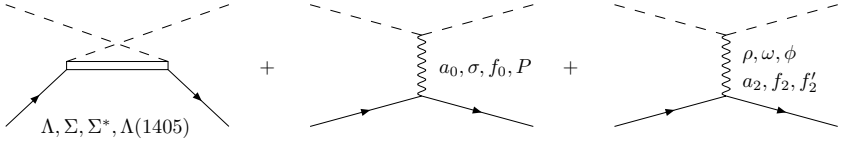

FIG. 10. Contributions to the K^+N potential from the u and t channel Feynman diagrams. External dashed and solid lines are always the K^+ and N, respectively.

TABLE VII. Isospin factors for the various exchanges for a given total isospin I of the K^+N system.

Exchange	$I=0$	$I=1$
$\sigma, f_0, \omega, \phi, f_2, f_2'$	1	1
a_0, ρ, a_2	−3	1
Λ	−1	1
Σ	3	1

used:

$$\begin{aligned}\mathcal{H}_{NNa_0} &= g_{NNa_0}(\bar{N}\boldsymbol{\tau}N)\cdot\boldsymbol{a}_0,\\ \mathcal{H}_{NN\sigma} &= g_{NN\sigma}\bar{N}N\sigma,\end{aligned} \tag{5.5}$$

$$\begin{aligned}\mathcal{H}_{KKa_0} &= g_{KKa_0}m_{\pi^+}\boldsymbol{a}_0\cdot(K^\dagger\boldsymbol{\tau}K),\\ \mathcal{H}_{KK\sigma} &= g_{\pi\pi\sigma}m_{\pi^+}\sigma K^\dagger K.\end{aligned} \tag{5.6}$$

The f_0 coupling is similar to the σ coupling. Besides the exchange of f_2 and f_2', the isovector tensor meson a_2 is also exchanged. The following tensor-meson couplings are used:

$$\begin{aligned}\mathcal{H}_{NNa_2} &= \left[\frac{iF_{1NNa_2}}{4}\bar{N}(\gamma_\mu\overleftrightarrow{\partial_\nu}+\gamma_\nu\overleftrightarrow{\partial_\mu})\boldsymbol{\tau}N\right.\\ &\quad\left.-\frac{F_{2NNa_2}}{4}\bar{N}\overleftrightarrow{\partial^\mu}\overleftrightarrow{\partial^\nu}\boldsymbol{\tau}N\right]\cdot\boldsymbol{a}_2^{\mu\nu},\\ \mathcal{H}_{NNf_2} &= \left[\frac{iF_{1NNf_2}}{4}\bar{N}(\gamma_\mu\overleftrightarrow{\partial_\nu}+\gamma_\nu\overleftrightarrow{\partial_\mu})N\right.\\ &\quad\left.-\frac{F_{2NNf_2}}{4}\bar{N}\overleftrightarrow{\partial^\mu}\overleftrightarrow{\partial^\nu}N\right]f_2^{\mu\nu},\end{aligned} \tag{5.7}$$

$$\begin{aligned}\mathcal{H}_{KKa_2} &= \frac{g_{KKa_2}}{m_{\pi^+}}\boldsymbol{a}_2^{\mu\nu}\cdot(\partial_\mu K^\dagger\boldsymbol{\tau}\partial_\nu K),\\ \mathcal{H}_{KKf_2} &= \frac{g_{KKf_2}}{m_{\pi^+}}f_2^{\mu\nu}(\partial_\mu K^\dagger\partial_\nu K).\end{aligned} \tag{5.8}$$

The coupling of f_2' is similar to the f_2 coupling. A repulsive contribution is obtained from Pomeron exchange, which is assumed to couple as a singlet, and the value of its coupling constant is determined in the πN system.

The isospin structure gives the isospin factors listed in Table VII, see also Appendix A. The spin-space amplitudes in paper I need to be multiplied by these isospin factors to find the complete K^+N amplitude.

Summarizing, we consider in the t channel the exchanges of the scalar mesons σ, f_0, and a_0, the Pomeron, the vector mesons ω, ϕ, and ρ, and the tensor mesons a_2, f_2, and f_2'; and in the u channel, the exchanges of the baryons Λ, Σ, $\Sigma(1385)(\Sigma^*)$, and $\Lambda(1405)(\Lambda^*)$.

The Coulomb interaction is neglected in the NSC model. Its contribution to the partial wave phase shifts is in principle relevant at very low energies. However, for the K^+N interaction, we will investigate not only the phase shifts, but also some scattering observables. The differential cross section and polarization in the $K^+p\to K^+p$ channel as a function of the scattering angle clearly show the effect of the Coulomb peak at forward angles: the differential cross sections blow up and the polarizations go to zero. For the description of these scattering observables we correct for the Coulomb interaction by replacing the spin-nonflip and spin-flip scattering amplitudes $\tilde{f}$ and $\tilde{g}$ in paper I by [4,45]

$$\begin{aligned}\tilde{f} &= \sum_L\left[(L+1)F_{L+\frac{1}{2},L}+LF_{L-\frac{1}{2},L}\right]e^{2i\phi_L}P_L(\cos\theta)+f_C,\\ \tilde{g} &= \sum_L\left[F_{L+\frac{1}{2},L}-F_{L-\frac{1}{2},L}\right]e^{2i\phi_L}\sin\theta\frac{dP_L(\cos\theta)}{d\cos\theta}.\end{aligned} \tag{5.9}$$

Here f_C is the Coulomb amplitude and ϕ_L are the Coulomb phase shifts defined, respectively, as

$$\begin{aligned}f_C &= -\frac{\alpha}{2kv\sin^2(\theta/2)}e^{-i\frac{\alpha}{v}\ln(\sin^2(\theta/2))},\\ \phi_L &= \sum_{n=1}^{L}\arctan\left(\frac{\alpha}{nv}\right),\end{aligned} \tag{5.10}$$

where k is the c.m. momentum, v is the relative velocity of the particles in the c.m. system, θ is the c.m. scattering angle, and α is the fine structure constant.

It is instructive to examine the relative strength of the different exchanges that contribute to the partial wave K^+N potentials. The on-shell potentials are given in Figs. 11 and 12 for each partial wave. The largest contribution comes from vector-meson exchange; ω exchange gives the largest contribution, and the isospin splitting of the vector mesons is

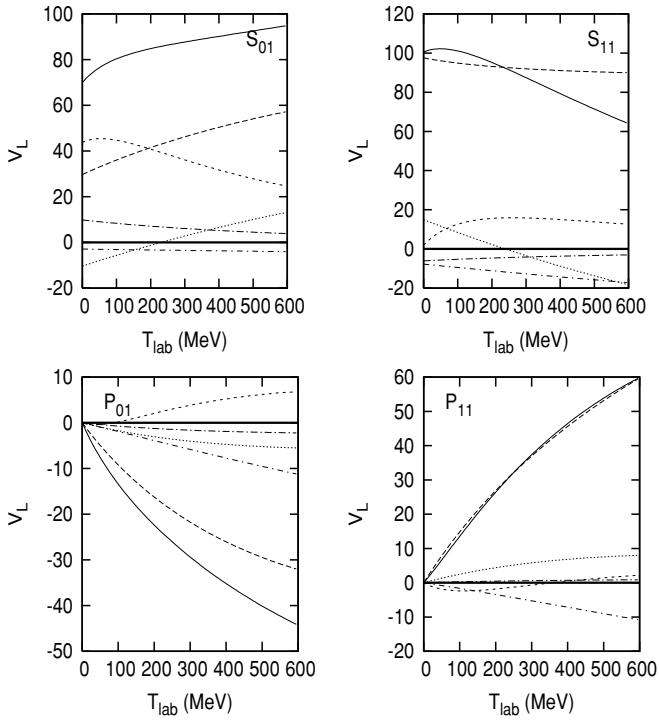

FIG. 11. Total K^+N S_{01}, S_{11}, P_{01}, and P_{11} partial wave potentials V_L as a function of $T_{\rm lab}$ are given by the solid line. The various contributions are (a) long dashed line: Vector mesons (b) short dashed line: Scalar mesons and Pomeron (c) dotted line: Λ and Σ (d) long dash-dotted line: Σ^* and Λ^* (e). short dash-dotted line: Tensor mesons.

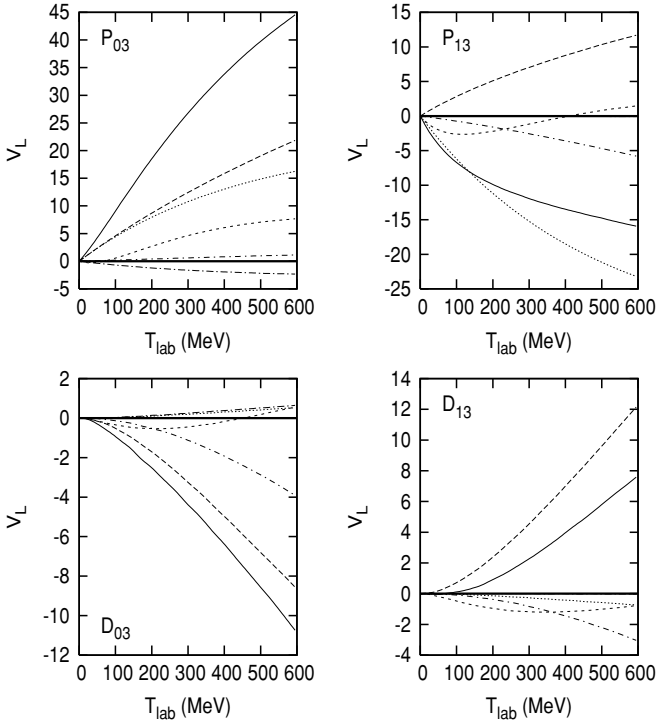

FIG. 12. As in Fig. 11, but for the P_{03}, P_{13}, D_{03}, and D_{13} partial wave potentials.

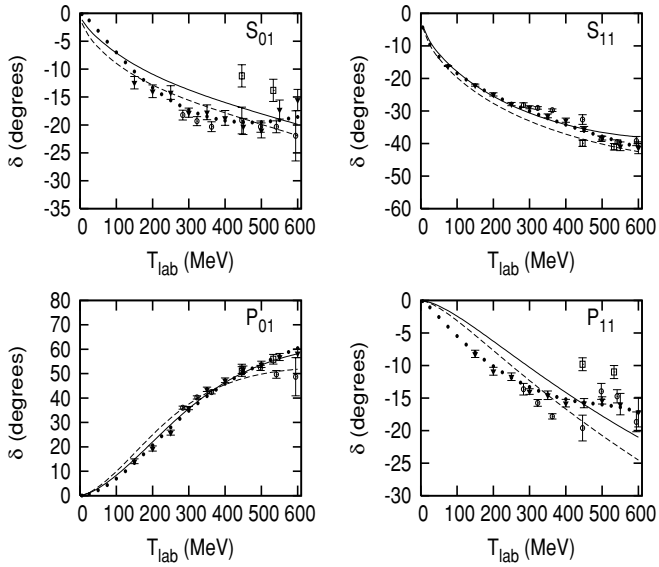

FIG. 13. S_{01}-, S_{11}-, P_{01}-, and P_{11}-wave K^+N phase shifts δ as a function of $T_{\rm lab}$. Empirical phases are from SP92 [44] multienergy phases (dots) and single-energy phases (filled triangles), [45] single-energy phases (open circles), and [46] single-energy phases (open squares). The NSC K^+N model is given by the solid line; the dashed line is the model without tensor mesons.

caused by ρ exchange. The S_{11}, P_{01}, and P_{11} partial waves are especially dominated by vector-meson exchange.

The cancellation between the scalar mesons and the Pomeron in the K^+N interaction is less than in the πN interaction, so the scalar mesons and the Pomeron give a relevant contribution. Specifically, a large repulsive contribution is seen in the S waves.

The contribution from Λ and Σ exchange is large in the $J = \frac{3}{2}$ P waves, and small in the other partial waves. This exchange plays in particular an important role in describing the rise of the P_{13} phase shift. The contribution of the strange resonances Σ^* and Λ^* is practically negligible over the whole energy range in most partial waves, except for the S_{01} and P_{03} partial waves.

The tensor mesons give a relevant contribution in most partial waves, especially at higher energies. The inclusion of tensor-meson exchange in the K^+N potential improved the description of the phase shifts at higher energies.

B. Results and discussion for K^+N scattering

We have fitted the NSC K^+N model to the energy-dependent SP92 partial wave analysis [44] up to kaon kinetic laboratory energy $T_{\rm lab} = 600$ MeV. The results of the fit are shown in Figs. 13 and 14. Table VIII shows the calculated and empirical S- and P-wave scattering lengths.

A reasonable agreement is obtained between the NSC K^+N model and the empirical phases up to $T_{\rm lab} = 600$ MeV, but the energy behavior of the empirical multienergy phases in the P_{11}, P_{03}, and D_{03} partial waves is not reproduced well by the NSC K^+N model. This, however, is also the case for the Jülich K^+N models [16,31]. The various phase shift analyses are not very consistent in these partial waves; in particular, the behavior of the SP92 multienergy P_{03} and D_{03} phases deviates much from the different single-energy phases. The low-energy structure of the multienergy D_{03} phase is not expected. One should wonder if this strange structure causes problems for other partial waves in the phase shift analysis.

The S-wave scattering lengths listed in Table VIII are reproduced well. For the P waves, the situation is less clear as the empirical P-wave scattering lengths found in the two partial wave analyses [44] and [47] are contradictory. The model P_{13} partial wave scattering length is in reasonable agreement with Ref. [44]. The P_{11} and P_{03} scattering lengths agree with Ref. [47].

Since the various phase shift analyses do not always give consistent results and one should wonder how well the multienergy SP92 phase shifts represent the experimental data, we also directly compared the NSC K^+N model with the experimental scattering observables. The total elastic cross

TABLE VIII. Calculated and empirical K^+N S-wave and P-wave scattering lengths in units of fm and fm^3.

Scat. length	Model	SP92 [44]	[47]	[27]
S_{01}	−0.09	0.00	−0.04	0.03 ± 0.15
S_{11}	−0.28	−0.33	−0.32	-0.30 ± 0.03
P_{01}	0.137	0.08	0.086	
P_{11}	−0.035	−0.16	−0.032	
P_{03}	−0.020	−0.13	−0.019	
P_{13}	0.059	0.07	0.021	

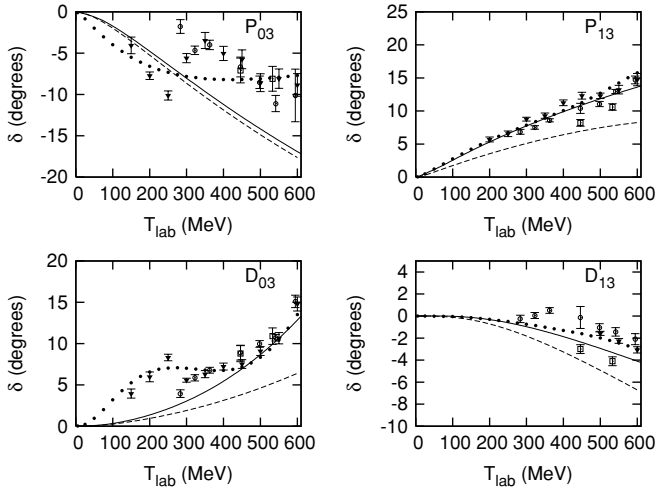

FIG. 14. As in Fig. 13, but for the P_{03}, P_{13}, D_{03}, and D_{13}-wave K^+N phase shifts.

sections as a function of $T_{\rm lab}$ are shown in Fig. 15. The experimental isospin-one (K^+p) total elastic cross section is known quite accurately; the isospin-zero total elastic cross section is known to less accuracy. The NSC K^+N model reproduces both total elastic cross sections quite well. The differential cross sections for the channels $K^+p \to K^+p$ and $K^+n \to K^+n$, having quite large error bars, are shown in Figs. 16 and 17 as a function of the scattering angle. They are described well by the NSC K^+N model. Finally,

TABLE IX. NSC K^+N-model parameters: Coupling constants, masses, and cutoff masses (MeV). Coupling constants with an asterisk were not searched in the fitting procedure, but constrained via $SU_f(3)$ or simply put to some value used in a previous work. $SU_f(3)$-breaking factors $\lambda_V = 0.764$ for the vector and $\lambda_S = 0.899$ for the scalar mesons were found.

Exchange	Coupling constants		Mass	Λ
ρ	$\frac{g_{NN\rho}g_{KK\rho}}{4\pi} = 0.667^*$	$\frac{f_{NN\rho}}{g_{NN\rho}} = 5.285$	770	1563
ω	$\frac{g_{NN\omega}g_{KK\omega}}{4\pi} = 2.572$	$\frac{f_{NN\omega}}{g_{NN\omega}} = 0.345$	783	1805
ϕ	$\frac{g_{NN\phi}g_{KK\phi}}{4\pi} = -0.573^*$	$\frac{f_{NN\phi}}{g_{NN\phi}} = 0.932^*$	1020	1563
a_0	$\frac{g_{NNa_0}g_{KKa_0}}{4\pi} = 3.461$		980	712
σ	$\frac{g_{NN\sigma}g_{KK\sigma}}{4\pi} = 20.676^*$		760	712
f_0	$\frac{g_{NNf_0}g_{KKf_0}}{4\pi} = 4.203^*$		975	712
a_2	$\frac{g_{NNa_2}g_{KKa_2}}{4\pi} = 0.019$	$\frac{f_{NNa_2}}{g_{NNa_2}} = -3.161$	1320	854
f_2	$\frac{g_{NNf_2}g_{KKf_2}}{4\pi} = 0.080$	$\frac{f_{NNf_2}}{g_{NNf_2}} = 0.382$	1270	854
f_2'	$\frac{g_{NNf_2'}g_{KKf_2'}}{4\pi} = 0.022^*$	$\frac{f_{NNf_2'}}{g_{NNf_2'}} = 3.393^*$	1525	854
Pom.	$\frac{g_{NNP}g_{KKP}}{4\pi} = 4.135^*$		315*	
Λ	$\frac{f^2_{\Lambda NK}}{4\pi} = 0.074^*$		1116	1029
Σ	$\frac{f^2_{\Sigma NK}}{4\pi} = 0.006^*$		1189	1029
Σ^*	$\frac{f^2_{\Sigma^* NK}}{4\pi} = 0.147^*$		1385	1052
Λ^*	$\frac{f^2_{\Lambda^* NK}}{4\pi} = 0.710^*$		1405	1052

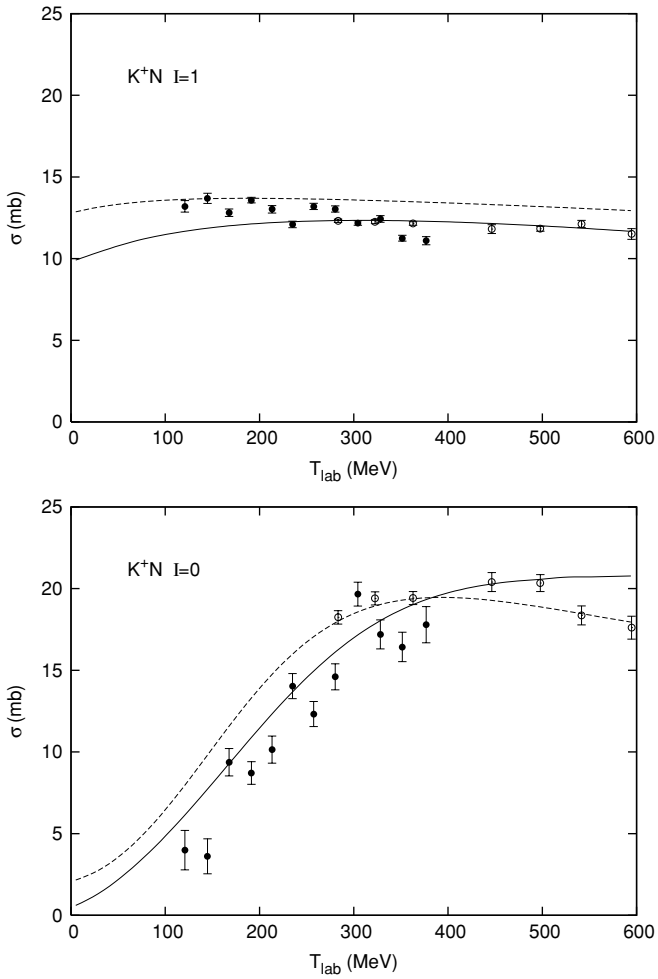

FIG. 15. Total elastic K^+N cross section σ as a function of $T_{\rm lab}$ for both isospin channels. Experimental cross sections are from Ref. [48] (full circles) and Ref. [45] (empty circles). The NSC K^+N model is given by the solid line; the dashed line is the model without tensor mesons.

the polarizations, also having large error bars, are given in Fig. 18 for the same channels as a function of the scattering angle. Again, a good agreement between the model and the experimental values is seen.

Although the empirical phase shifts are not very well described in some partial waves by the NSC K^+N model, the scattering observables as well as the S-wave scattering lengths are. The description of the experimental scattering data and the phase shifts by the NSC K^+N model, containing only one-particle-exchange processes, is as least as good as that of the Jülich models [16,31]. Those models, however, used two-particle exchanges to describe the experimental data.

The parameters of the NSC K^+N model searched and fixed in the fitting procedure are listed in Table IX. The NSC K^+N model has six different cutoff masses, which are free parameters in the fitting procedure. For the three scalar mesons we use the same cutoff mass; for the vector mesons, we use the same cutoff mass for ρ and ϕ, but allow for a different value for ω in order to find a better description of the S_{11} and P_{01} partial waves at higher energies. For the three tensor mesons necessary

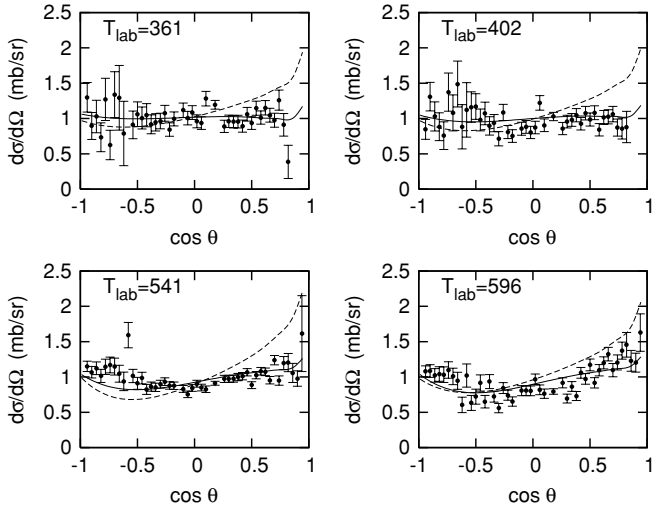

FIG. 16. $K^+p \to K^+p$ differential cross section $d\sigma/d\Omega$ as a function of $\cos\theta$, where θ is the c.m. scattering angle. Experimental differential cross sections are from Ref. [49]. The NSC K^+N model is given by the solid line; the dashed line is the model without tensor mesons.

to fit the S_{11}, P_{01}, and P_{13} partial waves simultaneously, we use the same cutoff mass. For the Pomeron mass, we take the value found for the NSC πN model; the meson and baryon masses have been fixed in the fitting procedure.

Ideal mixing is assumed for the vector mesons, so $\theta_V = 35.26^\circ$, and the $F/(F+D)$ ratios are fixed to the values in Ref. [52], $\alpha_V^e = 1.0$ and $\alpha_V^m = 0.275$. This fixes the PPV coupling constants in terms of the empirically determined $f_{\pi\pi\rho}$ and leaves $g_{NN\omega}$ and $f_{NN\omega}$ as fit parameters; the fitted values are in agreement with the literature. The tensor coupling $f_{NN\rho}$ is in principle determined in the NSC πN model; but since its value was determined to be very low we also fit this parameter in the NSC K^+N model, and we found a larger value for it there than in the NSC πN model. We note that the exchange of the vector meson ϕ is considered for consistency, but its contribution is negligible. For the scalar mesons, $g_{NN\sigma}$ and g_{NNf_0} are determined in the NSC πN model; we use g_{NNa_0} and θ_S as fit parameters, and all scalar-meson coupling constants are then determined. For the tensor mesons, we use the $F/(F+D)$ ratios $\alpha_T^e = 1.0$ and $\alpha_T^m = 0.4$ and an almost ideal mixing angle $\theta_T = 37.50^\circ$. This fixes the PPT coupling constants in terms of $f_{\pi\pi f_2}$. We notice that the tensor-meson coupling constants $g_T = \mathcal{M}F_1 + \mathcal{M}^2F_2$ and $f_T = -\mathcal{M}^2F_2$ are used in Table IX.

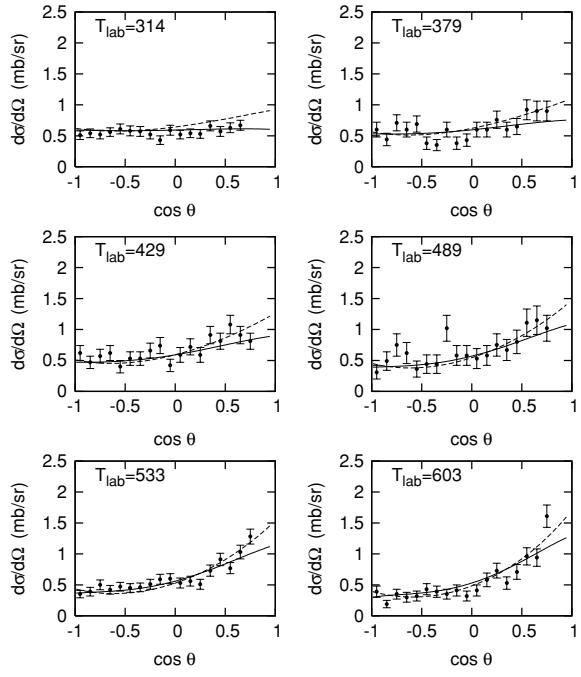

FIG. 17. $K^+n \to K^+n$ differential cross section $d\sigma/d\Omega$ as a function of $\cos\theta$, where θ is the c.m. scattering angle. Experimental differential cross sections are from Ref. [50]. The NSC K^+N model is given by the solid line; the dashed line is the model without tensor mesons.

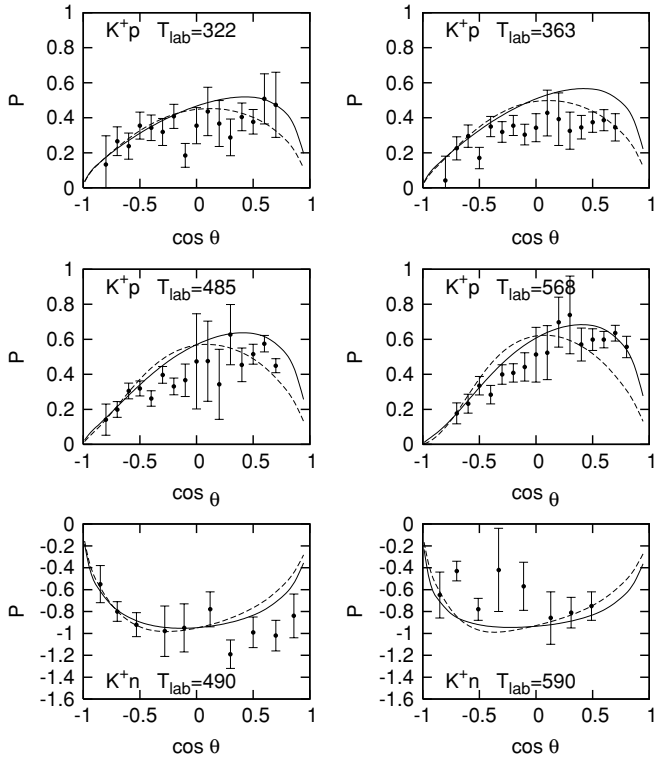

FIG. 18. $K^+p \to K^+p$ and $K^+n \to K^+n$ polarizations P as a function of $\cos\theta$, where θ is the c.m. scattering angle. The experimental polarizations are from Ref. [51]. The NSC K^+N model is given by the solid line; the dashed line is the model without tensor mesons.

The ΛNK and ΣNK coupling constants are determined by $f_{NN\pi}$ and fixing α_P at the value in Ref. [52] $\alpha_P = 0.355$. The Pomeron is considered as an $SU_f(3)$ singlet, and its coupling to the K^+N system is determined in the NSC πN model. For the Λ^* coupling constant, we take an average value from Ref. [36]. In the fitting procedure, we found that it was desirable to allow for an $SU_f(3)$ breaking for the scalar- and vector-meson couplings. The breaking factors we found are $\lambda_S = 0.899$ and $\lambda_V = 0.764$.

TABLE X. As in Table IX, but without tensor mesons and with $\lambda_V = 0.918$ and $\lambda_S = 0.900$.

Exchange	Coupling constants		Mass	Λ
ρ	$\frac{g_{NN\rho}g_{KK\rho}}{4\pi} = 0.641^*$	$\frac{f_{NN\rho}}{g_{NN\rho}} = 5.443$	770	1547
ω	$\frac{g_{NN\omega}g_{KK\omega}}{4\pi} = 2.215$	$\frac{f_{NN\omega}}{g_{NN\omega}} = 0.345$	783	1704
ϕ	$\frac{g_{NN\phi}g_{KK\phi}}{4\pi} = -0.243^*$	$\frac{f_{NN\phi}}{g_{NN\phi}} = 1.842^*$	1020	1547
a_0	$\frac{g_{NNa_0}g_{KKa_0}}{4\pi} = 3.806$		980	909
σ	$\frac{g_{NN\sigma}g_{KK\sigma}}{4\pi} = 26.068^*$		760	909
f_0	$\frac{g_{NNf_0}g_{KKf_0}}{4\pi} = 1.168^*$		975	909
Pom.	$\frac{g_{NNP}g_{KKP}}{4\pi} = 4.453^*$		296*	
Λ	$\frac{f^2_{\Lambda NK}}{4\pi} = 0.074^*$		1116	1041
Σ	$\frac{f^2_{\Sigma NK}}{4\pi} = 0.006^*$		1189	1041
Σ^*	$\frac{f^2_{\Sigma^* NK}}{4\pi} = 0.147^*$		1385	629
Λ^*	$\frac{f^2_{\Lambda^* NK}}{4\pi} = 0.710^*$		1405	629

The NSC K^+N model has 17 free physical parameters; 8 coupling constants, 1 mixing angle, 6 cutoff masses, and 2 $SU_f(3)$ breaking parameters. From the πN fit, we have $g_{NN\rho} = 0.78$ and $g_{NN\sigma} = 2.47$; from the K^+N fit, we have $g_{NN\omega} = 3.03$ and $g_{NNa_0} = 0.78$.

Besides the discussed NSC K^+N model, we also considered a model that does not contain tensor mesons. We fitted this model to the empirical phase shifts, and the results of the fit are given by the dashed lines in Figs. 13 and 14. The parameters of this model are listed in Table X. We observe that in the P_{13} and D_{03} partial waves, a noticeable difference can be seen between the two models. These partial waves as well as the S_{11} and P_{01} partial waves are described better by the NSC K^+N model, i.e., the model including the tensor mesons. The total cross sections and $K^+p \to K^+p$ differential cross sections are described better by the NSC K^+N model, while the $K^+n \to K^+n$ differential cross sections and the polarizations are described equally well by both models.

Summarizing, the NSC K^+N model gives a reasonable description of the empirical partial wave phase shifts and reproduces well the S-wave scattering lengths. The scattering observables, investigated because the various phase shift analyses are not always consistent, are described satisfactorily by this model.

C. Exotic resonances

Evidence for the existence of a resonance structure in the isospin-zero K^+N system at low energies has recently been found in various measurements from SPring-8, ITEP, Jefferson Lab, and ELSA [25]. The exotic resonance, a $qqqq\bar{q}$ state, was called Z^* but is now renamed as Θ^+. The experimental values for its mass and decay width are $\sqrt{s} \simeq 1540$ MeV and $\Gamma_{\Theta^+} \leqslant 25$ MeV. This is in good agreement with the theoretical predictions of Diakonov *et al.* [26] based on the chiral quark-soliton model, giving $\sqrt{s} \simeq 1530$ MeV and $\Gamma_{\Theta^+} \simeq 15$ MeV, isospin $I = 0$ and spin-parity $J^P = \frac{1}{2}^+$.

The present K^+N scattering data do not explicitly show this resonance structure, but some fluctuations in the isospin-zero scattering data around $\sqrt{s} = 1540$ MeV are present; however, the decay width of Θ^+ is expected to be quite small. Arndt *et al.* [53] have reanalyzed the K^+N scattering database and investigated the possibility of a resonance structure in their K^+N phase shift analysis. Since their last phase shift analysis [44], no new scattering data have become available. Arndt *et al.* concluded that the Θ^+ decay width must indeed be quite small in view of the present scattering data. They concluded that Γ_{Θ^+} is not much larger than a few MeV.

In this subsection the NSC K^+N model, describing well the experimental data far beyond the Θ^+ resonance region, is used to examine the influence of including this resonance explicitly on the total elastic isospin-zero K^+N cross section. This has also been done by the Jülich group [54]. The Θ^+ resonance is assumed to be present in the P_{01} partial wave. The procedure for including the Θ^+ resonance explicitly in the K^+N system is completely the same as for the Δ in the πN system. This renormalization procedure, giving a good description of the πN P_{33} partial wave, is described in detail in Sec. III.

A pole diagram for the Θ^+ resonance with bare mass and coupling constant M_0 and g_0 is added to the K^+N potential; iteration in the integral equation dresses the vertex and self-energy. The renormalization procedure ensures a pole at the physical Θ^+ mass and the vanishing of the self-energy and its first derivative at the pole position. The bare mass and coupling constant are in the renormalization procedure determined in terms of the physical parameters. The physical $KN\Theta^+$ coupling constant is calculated using the decay width and Eq. (4.8). We did not fit the model which includes the Θ^+ resonance to the scattering data, but simply used the NSC K^+N model, added the Θ^+ pole diagram, and observed the change in the cross section.

The total elastic cross section in the isospin-zero channel, predicted by the NSC K^+N model, is given in Fig. 19 by the

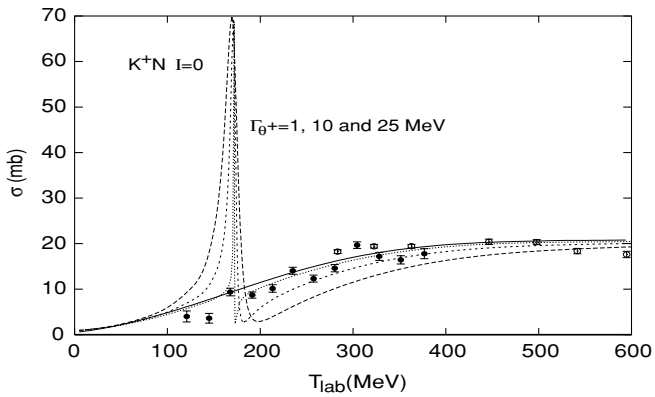

FIG. 19. Θ^+ resonance included in the NSC K^+N model. The total elastic K^+N cross section σ is given as a function of $T_{\rm lab}$. The experimental cross sections are from Ref. [48] (full circles) and Ref. [45] (empty circles). The NSC K^+N model is given by the solid line. The dotted, short, and long dashed curves correspond to $\Gamma_{\theta^+} = 1$, 10, and 25 MeV, respectively.

solid line. Inclusion of the Θ^+ resonance results in a peak in the isospin-zero cross section around $\sqrt{s} = 1540$ MeV or $T_{\rm lab} = 171$ MeV. We calculated the influence of the Θ^+ resonance on the isospin-zero cross section for three values of its decay width, $\Gamma_{\Theta^+} = 1$, 10, and 25 MeV.

Far from the resonance position, the dashed curves coincide with the solid NSC K^+N curve. It is clear that the smaller the Θ^+ decay width, the narrower the peak and the more the dashed curve coincides with the solid NSC K^+N curve. It is hard to reconcile the present isospin-zero K^+N scattering data with a Θ^+ resonance decay width larger than 10 MeV, unless the Θ^+ resonance lies much closer to threshold, where no scattering data are available. In both cases, new and accurate scattering experiments, especially at low energies and around $\sqrt{s} = 1540$ MeV, would be desirable.

VI. SUMMARY AND OUTLOOK

In paper I the NSC model was derived. Its application to the πN interaction presented in this paper shows that the soft-core approach of the Nijmegen group gives a good description of not only the *NN* and *YN* data, but also the πN data. The NSC πN model serves as a solid basis for the NSC K^+N model, assumed to be connected via $\mathrm{SU}_f(3)$ symmetry.

In the πN cross section, some resonances are present at low and intermediate energies, e.g., the Δ and the Roper. It turned out that these resonances cannot be described by using only a πN potential; i.e., they could not be generated dynamically. This confirms the quark-model picture. We consider these resonances as, at least partially, genuine three-quark states, and we treat them in the same way as the nucleon. Therefore, we have included *s*-channel diagrams for these resonances in the NSC πN model. However, this is done carefully in a renormalized procedure, i.e., a procedure in which physical coupling constants and masses are used.

The NSC πN model contains the *s*- and *u*-channel exchanges of the baryons N, Δ, Roper, and S_{11} and the *t*-channel exchanges of the scalar mesons σ and f_0, vector meson ρ, and tensor mesons f_2 and f_2'. An excellent fit to the empirical *S*- and *P*-wave phase shifts up to pion laboratory energy 600 MeV is given in Sec. IV. We found normal values for the coupling constants and cutoff masses, except for a low value of $f_{NN\rho}/g_{NN\rho}$, which is also a problem in other πN models. The scattering lengths have been reproduced well. The soft-pion theorems for low-energy πN scattering are satisfied, since the *S*-wave scattering lengths are described well. The c_1, c_2, c_3, and c_4 terms in chiral perturbation theory are described implicitly by the NSC πN model, higher derivative terms in chiral perturbation theory are effectively described by the propagators and Gaussian form factors in the NSC πN model.

The NSC K^+N model and the fit to the experimental data are presented in Sec. V. The model contains the *u*-channel exchanges of the baryons Λ, Σ, Σ^*, and Λ^* and the *t*-channel exchanges of the scalar mesons a_0, σ, and f_0, the vector mesons ρ, ω, and ϕ, and the tensor mesons a_2, f_2, and f_2'. The quality of the fit to the empirical phase shifts up to kaon laboratory energy 600 MeV is not as good as for the NSC πN model, but the NSC K^+N model certainly reflects the present state of the art. The scattering observables and the *S*-wave scattering lengths are reproduced well.

Low-energy (exotic) resonances have never been seen in the present K^+N scattering data; however, indications for the existence of a narrow resonance in the isospin-zero K^+N system have been found recently in several photoproduction experiments. We have included this resonance $\Theta^+(1540)$ in the NSC K^+N model, in the same way as we included resonances in the NSC πN models, and investigated its influence as a function of its decay width on the total cross section. We concluded that in view of the present scattering data, its decay width must be smaller than 10 MeV.

The present NSC πN and K^+N models could be improved by adding two-particle-exchange processes to the πN and K^+N potentials, similar to the extended soft-core *NN* and *YN* models. Also, the Coulomb interaction, which in principle plays a role at very low energies, has not been considered here.

Finally, this work provides the basis for extending the soft-core approach to the antikaon-nucleon ($\bar{K}N$) interaction and to meson-baryon interactions in general. The $\bar{K}N$ system is already at threshold coupled to the $\Lambda\pi$ and $\Sigma\pi$ channels. The coupled channels treatment for this system is similar to that of the *YN* system.

ACKNOWLEDGMENTS

The authors thank Prof. J. J. de Swart and Prof. R. G. E. Timmermans for stimulating discussions.

APPENDIX: OBE AND BARYON-EXCHANGE ISOSPIN FACTORS

We outline the calculation of the isospin factors for the meson-baryon interactions, making use of the Wigner 6-*j* and 9-*j* symbols in Ref. [55]; this reference also gives relations for interchanging the labels of Clebsch-Gordan coefficients. Examples for the πN and K^+N interactions are given.

A. Baryon exchange in πN interactions

The isospin matrix element for a given total final and initial isospin in the πN system reads

$$\langle I_f M_f|\mathcal{H}|I_i M_i\rangle = C^{1\ \frac{1}{2}\ I_f}_{m'\ n'\ M_f} C^{1\ \frac{1}{2}\ I_i}_{m\ n\ M_i} \langle \pi_{m'} N_{n'}|\mathcal{H}|\pi_m N_n\rangle, \quad \text{(A1)}$$

where I is the total isospin of the system and M its z component, m is the z component of the pions isospin, and n is the z component of the nucleons isospin, see Fig. 20. We can

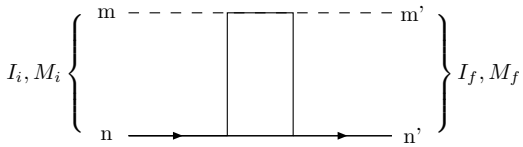

FIG. 20. Matrix element for the total isospin; m is the z component of the pion isospin and n is the z component of the nucleon isospin.

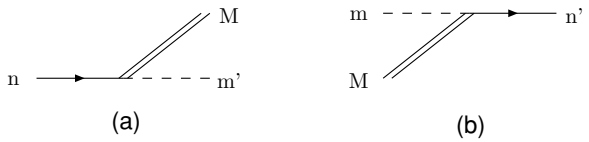

FIG. 21. (a) Baryon emission vertex. (b) Baryon absorption vertex.

rewrite the first Clebsch-Gordan coefficient in Eq. (A1) [55] as

$$C^{1\ \frac{1}{2}\ I_f}_{m'\ n'\ M_f} = (-)^{\frac{3}{2}-I_f} C^{\frac{1}{2}\ 1\ I_f}_{n'\ m'\ M_f}. \tag{A2}$$

For baryon exchange, the isospin interaction Hamiltonian $\mathcal{H}$ for either the $NN\pi$ or the $N\Delta\pi$ vertex is

$$\mathcal{H} = \langle i||T'||1/2\rangle C^{\frac{1}{2}\ 1\ i}_{n\ m\ M}[\psi^*_M N_n \pi^*_m + N^*_n \psi_M \pi_m], \tag{A3}$$

where ψ_M denotes either the nucleon with $i = \frac{1}{2}$ or the Δ with $i = \frac{3}{2}$, and T' denotes $\boldsymbol{\tau}$ or $\boldsymbol{T}$. Here $\pi_{+1} = -(\pi_1 + i\pi_2)/\sqrt{2}$, $\pi_{-1} = (\pi_1 - i\pi_2)/\sqrt{2}$ and $\pi_0 = \pi_3$. We note that $\pi_m = (-)^m \pi^*_{-m}$. The baryon emission vertex shown in Fig. 21 gives, besides the reduced matrix element, the factor

$$(-)^{m'} C^{\frac{1}{2}\ 1\ i}_{n\ -m'\ M} = (-)^{2i-M-\frac{1}{2}} \sqrt{\frac{2i+1}{3}} C^{\frac{1}{2}\ i\ 1}_{n\ -M\ m'}. \tag{A4}$$

The baryon absorption vertex shown in Fig. 21 gives, besides the reduced matrix element, the factor

$$(-)^m C^{\frac{1}{2}\ 1\ i}_{n'\ -m\ M} = -\sqrt{\frac{2i+1}{2}} C^{1\ i\ \frac{1}{2}}_{m\ M\ n'}. \tag{A5}$$

Using Eqs. (A2), (A4), and (A5), we find for the total isospin matrix element of Eq. (A1)

$$\begin{aligned}\langle I_f M_f|\mathcal{H}|I_i M_i\rangle &= (-)^{1+3i-I_f+(i-M)} \frac{2i+1}{\sqrt{6}} \\ &\times C^{\frac{1}{2}\ 1\ I_f}_{n'\ m'\ M_f} C^{1\ \frac{1}{2}\ I_i}_{m\ n\ M_i} \\ &\times C^{\frac{1}{2}\ i\ 1}_{n\ -M\ m'} C^{1\ i\ \frac{1}{2}}_{m\ M\ n'} \\ &\times \langle i||T'||1/2\rangle^2. \end{aligned} \tag{A6}$$

Using the identity $(-)^{i-M} = \sqrt{2i+1} C^{i\ i\ 0}_{M\ -M\ 0}$, we find

$$\begin{aligned}\langle I_f M_f|\mathcal{H}|I_i M_i\rangle &= (-)^{1+3i-I_f} \sqrt{\frac{2i+1}{6}} (2i+1) \\ &\times \langle i||T'||1/2\rangle^2 \begin{bmatrix} 1 & i & \frac{1}{2} \\ \frac{1}{2} & i & 1 \\ I & 0 & I \end{bmatrix} \\ &= -(2i+1)\langle i||T'||1/2\rangle^2 \\ &\times \begin{Bmatrix} \frac{1}{2} & 1 & i \\ \frac{1}{2} & 1 & I \end{Bmatrix}. \end{aligned} \tag{A7}$$

TABLE XI. Isospin factors for nucleon and Δ exchanges for a given total isospin I of the πN system.

Exchange	$I = \frac{1}{2}$	$I = \frac{3}{2}$
N	-1	2
Δ	$\frac{4}{3}$	$\frac{1}{3}$

Here, we use the conservation of isospin $I_f = I_i = I$. For nucleon exchange, the reduced matrix element is $\langle \frac{1}{2}\|\boldsymbol{\tau}\|\frac{1}{2}\rangle = \sqrt{3}$; for Δ exchange, it is $\langle \frac{3}{2}\|\boldsymbol{T}\|\frac{1}{2}\rangle = 1$. The isospin factors are given in Table XI.

B. ρ exchange in K^+N interactions

The isospin matrix element for a given total final and initial isospin in the K^+N system reads

$$\begin{aligned}\langle I_f M_f|\mathcal{H}|I_i M_i\rangle &= C^{\frac{1}{2}\ \frac{1}{2}\ I_f}_{m'\ n'\ M_f} C^{\frac{1}{2}\ \frac{1}{2}\ I_i}_{m\ n\ M_i} \\ &\times \langle K_{m'} N_{n'}|\mathcal{H}|K_m N_n\rangle, \end{aligned} \tag{A8}$$

where I is the total isospin of the system and M its z component, m is the z component of the kaon isospin, and n is the z component of the nucleon isospin. For ρ exchange, the isospin interaction Hamiltonians $\mathcal{H}$ for the $NN\rho$ and $KK\rho$ vertex are

$$\begin{aligned}\mathcal{H}_{NN\rho} &= \sqrt{3} C^{\frac{1}{2}\ 1\ \frac{1}{2}}_{n\ M\ n'} N^*_{n'} N_n \rho^*_M, \\ \mathcal{H}_{KK\rho} &= \sqrt{3} C^{\frac{1}{2}\ 1\ \frac{1}{2}}_{m\ M\ m'} K^*_{m'} K_m \rho^*_M. \end{aligned} \tag{A9}$$

Note that $\rho_m = (-)^m \rho^*_{-m}$. The ρ emission vertex shown in Fig. 22 gives the factor

$$\sqrt{3}(-)^{-M} C^{\frac{1}{2}\ 1\ \frac{1}{2}}_{n\ -M\ n'}. \tag{A10}$$

The ρ absorption vertex shown in Fig. 22 gives the factor

$$\sqrt{3} C^{\frac{1}{2}\ 1\ \frac{1}{2}}_{m\ M\ m'}. \tag{A11}$$

Using Eqs. (A9), (A10), and (A11), we find for the total isospin matrix element of Eq. (A8)

$$\langle I_f M_f|\mathcal{H}|I_i M_i\rangle = (-)^{-M} 3 C^{\frac{1}{2}\ \frac{1}{2}\ I_f}_{m'\ n'\ M_f} C^{\frac{1}{2}\ \frac{1}{2}\ I_i}_{m\ n\ M_i} C^{\frac{1}{2}\ 1\ \frac{1}{2}}_{n\ -M\ n'} C^{\frac{1}{2}\ 1\ \frac{1}{2}}_{m\ M\ m'}. \tag{A12}$$

Applying the identity $(-)^{-M} = -\sqrt{3} C^{1\ 1\ 0}_{-M\ M\ 0}$, we find

$$\langle I_f M_f|\mathcal{H}|I_i M_i\rangle = -3\sqrt{3} \begin{bmatrix} \frac{1}{2} & 1 & \frac{1}{2} \\ \frac{1}{2} & 1 & \frac{1}{2} \\ I & 0 & I \end{bmatrix} = 2I\,(I+1) - 3. \tag{A13}$$

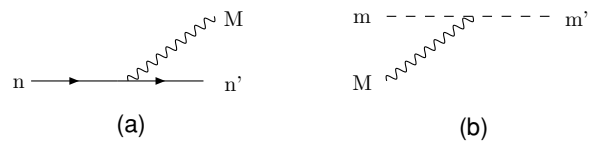

FIG. 22. (a) ρ emission vertex. (b) ρ absorption vertex.

Here, we use the conservation of isospin $I_f = I_i = I$. For $I = 0$, we find an isospin factor of -3; for $I = 1$, a factor of 1. Other isospin factors can be calculated in the same way; all relevant isospin factors for the πN and K^+N interaction are listed in Tables I and VII, respectively.

[1] H. Polinder and T. A. Rijken, Phys. Rev. C, accepted for publication, 2005.
[2] G. F. Chew and F. E. Low, Phys. Rev. **101**, 1570 (1956).
[3] J. Hamilton, in *High Energy Physics*, edited by E. H. S. Burhop (Academic Press Inc., New York, 1967), Vol. 1.
[4] B. H. Bransden and R. G. Moorhouse, *The Pion-Nucleon System* (Princeton University, Princeton, NJ, 1973).
[5] G. Höhler, F. Kaiser, R. Koch, and E. Pietarinen, *Handbook of Pion-Nucleon Scattering* (Fachinformationszentrum Energie, Physik, Mathematik, Karlsruhe, 1979); G. Höhler, *Elastic and Charge Exchange Scattering of Elementary Particles. Vol. B. Pion Nucleon Scattering. Pt. 2. Methods and Results of Phenomenological Analyses* (Springer-Verlag, Berlin, 1983).
[6] T. A. Rijken, H. Polinder, and J. Nagata, Phys. Rev. C **66**, 044008 (2002); **66**, 044009 (2002); T. A. Rijken, V. G. J. Stoks, and Y. Yamamoto, *ibid.* **59**, 21 (1999); B. Holzenkamp, K. Holinde, and J. Speth, Nucl. Phys. **A500**, 485 (1989); A. Reuber, K. Holinde, and J. Speth, *ibid.* **A570**, 543 (1994).
[7] R. Machleidt, K. Holinde, and C. Elster, Phys. Rep. **149**, 1 (1987).
[8] B. C. Pearce and B. K. Jennings, Nucl. Phys. **A528**, 655 (1990).
[9] F. Gross and Y. Surya, Phys. Rev. C **47**, 703 (1993).
[10] G. Schütz, J. W. Durso, K. Holinde, and J. Speth, Phys. Rev. C **49**, 2671 (1994).
[11] G. Schütz, K. Holinde, J. Speth, B. C. Pearce, and J. W. Durso, Phys. Rev. C **51**, 1374 (1995).
[12] T. Sato and T.-S. H. Lee, Phys. Rev. C **54**, 2660 (1996); A. D. Lahiff and I. R. Afnan, *ibid.* **60**, 024608 (1999).
[13] V. Pascalutsa and J. A. Tjon, Phys. Rev. C **61**, 054003 (2000).
[14] A. M. Gasparyan, J. Haidenbauer, C. Hanhart, and J. Speth, Phys. Rev. C **68**, 045207 (2003).
[15] R. Büttgen, K. Holinde, A. Müller-Groeling, J. Speth, and P. Wyborny, Nucl. Phys. **A506**, 586 (1990).
[16] M. Hoffmann, J. W. Durso, K. Holinde, B. C. Pearce, and J. Speth, Nucl. Phys. **A593**, 341 (1995).
[17] H. M. Nieland and J. A. Tjon, Phys. Lett. **B27**, 309 (1968); H. M. Nieland, Ph.D. thesis, University of Nijmegen, 1971.
[18] D. Lu, S. C. Phatak, and R. H. Landau, Phys. Rev. C **51**, 2207 (1995).
[19] J. Gasser, H. Leutwyler, M. P. Locher, and M. E. Sainio, Phys. Lett. **B213**, 85 (1988); V. Bernard, N. Kaiser, and U.-G. Meißner, Nucl. Phys. **A615**, 483 (1997); N. Fettes, U.-G. Meißner, and S. Steininger, *ibid.* **A640**, 199 (1998); U.-G. Meißner and J. A. Oller, *ibid.* **A673**, 311 (2000); N. Fettes and U.-G. Meißner, *ibid.* **A676**, 311 (2000); **A693**, 693 (2001); A. Datta and S. Pakvasa, Phys. Rev. D **56**, 4322 (1997).
[20] M. F. M. Lutz and E. E. Kolomeitsev, Nucl. Phys. **A700**, 193 (2002).
[21] R. A. Arndt, I. I. Strakovsky, R. L. Workman, and M. M. Pavan, Phys. Rev. C **52**, 2120 (1995).
[22] R. A. Arndt, W. J. Briscoe, I. I. Strakovsky, R. L. Workman, and M. M. Pavan, Phys. Rev. C **69**, 035213 (2004).
[23] R. Koch and E. Pietarinen, Nucl. Phys. **A336**, 331 (1980).
[24] J. R. Carter, D. V. Bugg, and A. A. Carter, Nucl. Phys. **B58**, 378 (1973).
[25] T. Nakano *et al.*, Phys. Rev. Lett. **91**, 012002 (2003); S. Stepanyan *et al.*, *ibid.* **91**, 252001 (2003); V. V. Barmin *et al.*, Phys. Atom. Nucl. **66**, 1715 (2003); J. Barth *et al.*, Phys. Lett. **B572**, 127 (2003).
[26] D. Diakonov, V. Petrov, and M. Polyakov, Z. Phys. A **359**, 305 (1997).
[27] C. B. Dover and G. E. Walker, Phys. Rep. **89**, 1 (1982).
[28] T. Barnes and E. S. Swanson, Phys. Rev. C **49**, 1166 (1994).
[29] B. Silvestre-Brac, J. Leandri, and J. Labarsouque, Nucl. Phys. **A589**, 585 (1995); B. Silvestre-Brac, J. Labarsouque, and J. Leandri, *ibid.* **A613**, 342 (1997).
[30] S. Lemaire, J. Labarsouque, and B. Silvestre-Brac, Nucl. Phys. **A696**, 497 (2001); **A700**, 330 (2002).
[31] D. Hadjimichef, J. Haidenbauer, and G. Krein, Phys. Rev. C **66**, 055214 (2002).
[32] F. E. Low, Phys. Rev. D **12**, 163 (1975); S. Nussinov, Phys. Rev. Lett. **34**, 1286 (1975).
[33] S. Weinberg, Phys. Rev. Lett. **17**, 616 (1966); S. L. Adler, Phys. Rev. **137**, AB4 (1965).
[34] J. J. de Swart, T. A. Rijken, P. M. Maessen, and R. G. E. Timmermans, Nuovo Cimento A **102**, 203 (1989).
[35] J. J. de Swart, Rev. Mod. Phys. **35**, 916 (1963).
[36] M. M. Nagels, T. A. Rijken, and J. J. de Swart, Nucl. Phys. **B147**, 189 (1979).
[37] R. W. Haymaker, Phys. Rev. **181**, 2040 (1969).
[38] V. Pascalutsa, Ph.D. thesis, University of Utrecht, 1998.
[39] M. I. Haftel and F. Tabakin, Nucl. Phys. **A158**, 1 (1970).
[40] P. A. Carruthers, *Spin and Isospin in Particle Physics* (Gordon and Breach, New York, 1971), the isospin-$\frac{1}{2}$ isospin-$\frac{3}{2}$ transition operator we use is equal to $1/\sqrt{2}$ times the operator defined in this reference.
[41] M. M. Nagels, T. A. Rijken, and J. J. de Swart, Phys. Rev. D **12**, 744 (1975).
[42] H. Pilkuhn, *The Interactions of Hadrons* (North-Holland, Amsterdam, 1967).
[43] M. M. Nagels, T. A. Rijken, and J. J. de Swart, Phys. Rev. D **17**, 768 (1978).
[44] J. S. Hyslop, R. A. Arndt, L. D. Roper, and R. L. Workman, Phys. Rev. D **46**, 961 (1992).
[45] K. Hashimoto, Phys. Rev. C **29**, 1377 (1983).
[46] S. J. Watts *et al.*, Phys. Lett. **B95**, 323 (1980).
[47] B. R. Martin, Nucl. Phys. **B94**, 413 (1975).
[48] T. Bowen, P. K. Caldwell, F. N. Dikmen, E. W. Jenkins, R. M. Kalbach, D. V. Petersen, and A. E. Pifer, Phys. Rev. D **2**, 2599 (1970).
[49] B. J. Charles *et al.*, Nucl. Phys. **B131**, 7 (1977).
[50] G. Giacomelli *et al.*, Nucl. Phys. **B56**, 346 (1973).
[51] B. R. Lovett, V. W. Hughes, M. Mishina, M. Zeller, D. M. Lazarus, and I. Nakano, Phys. Rev. D **23**, 1924 (1981); A. W. Robertson *et al.*, Phys. Lett. **B91**, 465 (1980).

[52] P. M. M. Maessen, T. A. Rijken, and J. J. de Swart, Phys. Rev. C **40**, 2226 (1989).

[53] R. A. Arndt, I. I. Strakovsky, and R. L. Workman, Phys. Rev. C **68**, 042201 (2003).

[54] J. Haidenbauer and G. Krein, Phys. Rev. C **68**, 052201 (2003); A. Sibirtsev, J. Haidenbauer, S. Krewald, and U.-G. Meißner, Phys. Lett. **B599**, 230 (2004); Eur. Phys. J. A **23**, 491 (2005).

[55] A. R. Edmonds, *Angular Momentum in Quantum Mechanics* (Princeton University, Princeton, NJ, 1957); the explicit relation between our $9j$ symbols and those of this reference's Eq. (6.4.4) is [56]

$$\begin{bmatrix} j_{11} & j_{12} & j_{13} \\ j_{21} & j_{22} & j_{23} \\ j_{31} & j_{32} & j_{33} \end{bmatrix} = [(2j_{13}+1)(2j_{31}+1)(2j_{23}+1) \times (2j_{32}+1)]^{1/2} \begin{Bmatrix} j_{11} & j_{12} & j_{13} \\ j_{21} & j_{22} & j_{23} \\ j_{31} & j_{32} & j_{33} \end{Bmatrix}.$$

[56] L. J. A. M. Somers, Ph.D. thesis, University of Nijmegen, 1984.